Analytica Chimica Acta xxx (2014) xxx–xxx

Contents lists available at ScienceDirect

Analytica Chimica Acta

journal homepage: www.elsevier.com/locate/aca

Review

Interactions of DNA with graphene and sensing applications of graphene field-effect transistor devices: A review

Nathaniel S. Green, Michael L. Norton *

Department of Chemistry, Marshall University, One John Marshall Drive, Huntington, WV 25755, United States

HIGHLIGHTS

- The interaction of DNA, including DNA nanostructures, and graphene is reviewed.
- Comparison of DNA graphene field-effect transistor (GFET) with other detection methods.
- Discussion of challenges present in the detection mechanism of GFETs.
- Use of DNA aptamer GFET sensors for the detection of small molecules and proteins.

GRAPHICAL ABSTRACT

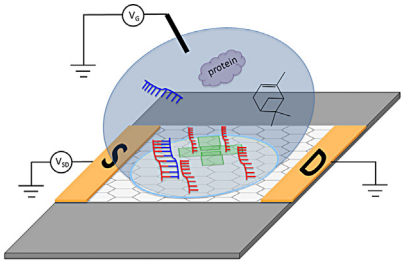

ARTICLE INFO

Article history:
Received 26 July 2014
Received in revised form 11 October 2014
Accepted 14 October 2014
Available online xxx

Keywords:
DNA aptamer
Graphene field-effect transistor
DNA origami
Biosensor
Small molecule detection

ABSTRACT

Graphene field-effect transistors (GFET) have emerged as powerful detection platforms enabled by the advent of chemical vapor deposition (CVD) production of the unique atomically thin 2D material on a large scale. DNA aptamers, short target-specific oligonucleotides, are excellent sensor moieties for GFETs due to their strong affinity to graphene, relatively short chain-length, selectivity, and a high degree of analyte variability. However, the interaction between DNA and graphene is not fully understood, leading to questions about the structure of surface-bound DNA, including the morphology of DNA nanostructures and the nature of the electronic response seen from analyte binding. This review critically evaluates recent insights into the nature of the DNA graphene interaction and its affect on sensor viability for DNA, small molecules, and proteins with respect to previously established sensing methods. We first discuss the sorption of DNA to graphene to introduce the interactions and forces acting in DNA based GFET devices and how these forces can potentially affect the performance of increasingly popular DNA aptamers and even future DNA nanostructures as sensor substrates. Next, we discuss the novel use of GFETs to detect DNA and the underlying electronic phenomena that are typically used as benchmarks for characterizing the analyte response of these devices. Finally, we address the use of DNA aptamers to increase the selectivity of GFET sensors for small molecules and proteins and compare them with other, state of the art, detection methods.

Abbreviations: GFET, graphene field-effect transistor; CVD, chemical vapor deposition; 2D, two-dimensional; DNA, deoxyribonucleic acid; SMFS, single molecule force microscopy; ssDNA, single-stranded deoxyribonucleic acid; AFM, atomic force microscopy; dsDNA, double-stranded deoxyribonucleic acid; PDGF, platelet derived growth factor; SAMs, self-assembled monolayers; HOPG, highly ordered pyrolytic graphite; SA, streptavidin; GO, graphene oxide; RIE, reactive ion etching; rGO, reduced graphene oxide; XPS, X-ray photoelectron spectroscopy; NrGO, nitrogen doped graphene oxide; V_{CNP}, conductance neutral point; LOD, limit of detection; GCE, glassy carbon electrode; ppm, parts per million; ppb, parts per billion; MIPK, methyl isopropyl ketone; CMUT, capacitive micromachined ultrasonic transducer; DMMP, dimethyl methylphosphonate; ATP, adenosine triphosphate; TMN, tris magnesium sodium buffer; PBS, phosphate buffered saline; DPV, differential pulse voltammetry; SERS, surface enhanced Raman spectroscopy; FET, field-effect transistor; PA, protective antigen; pI, isoelectric point; PBASE, pyrenebutanoic acid succinimidyl ester; TBA, thrombin binding aptamer; DAN, 1,5-diaminonapthalene; VGEF, vascular endothelial growth factor; MES, 2-(*N*-morpholino)ethanesulfonic acid; IgE, immunoglobulin E.

* Corresponding author. Tel.: +1 304 696 6627; fax: +1 304 696 3243.
E-mail address: norton@marshall.edu (M.L. Norton).

http://dx.doi.org/10.1016/j.aca.2014.10.023
0003-2670/

Contents

Nathaniel Green is a postdoctoral fellow in the Department of Chemistry at Marshall University. He obtained his Ph.D. in Organic Chemistry from the University of Oklahoma in 2013, working in the area of metal-enhanced fluorescence by studying the interaction of dye-doped silica nanoparticles and gold nanostructures. His current research interests are in the areas of inorganic and bionanostructuctures for applications in sensing, microscopy and microfluidics. His research work is exploring modified functional surfaces for DNA nanostructure deposition en route to developing multiplexed sensors within microfluidic devices.

Michael Norton is a Professor of Chemistry at Marshall University. He obtained his Ph.D. in Solid State Chemistry from Arizona State University in 1982, working in the area of two-dimensional magnetic materials. As a NRC postdoctoral researcher, he worked briefly in the area of oxide materials at the Naval Weapons Center at China Lake, California. As an assistant professor at the University of Georgia, he developed methods for electrochemical growth of superconducting oxide superlattices. In his career at Marshall University, his studies have focused on soft matter structures, including DNA based nanostructures, with emphasis on the fabrication and characterization of electro-optical nanoarchitecture for sensing applications.

1. Introduction

Graphene, or two-dimensional sheets of sp^2 hybridized carbon, devices have recently been realized, enabled by advances in the chemical vapor deposition (CVD) technique for growing large, wafer-scale layers of the material [1]. The unique electronic properties of graphene make it an enticing sensor material, particularly in view of its sensitive ambipolar nature (ability to be both p and n-type), which can be changed with applied fields or by charged species near the surface [2–4]. One such application is the use of graphene in field-effect transistors (FETs). A FET is a type of transistor device or electronic valve in which the conductivity of a length of uniform material (in this case graphene) changes its conductivity depending on the value of an externally applied electric field [5,6]. Because the number and type of carriers in graphene can be changed by this gate electric field, graphene FETs are called ambipolar [7]. The application of charged probe molecules to the surface (channel) modifies the graphene field-effect transistor (GFET) sensors' characteristics due to its sensitivity to external electric fields.

Thus, graphene field-effect transistor (GFET) sensors' functionality has been realized by the application of probe molecules to the surface. DNA aptamers, target-specific oligonucleotides, are highly selective probes that have been widely used in sensing applications for multiple analytes [8,9]. However, applying DNA aptamers to the surface of graphene presents unique challenges and opportunities given the complicated interactions between the biopolymers and these carbonaceous substrates. These interactions are further complicated by the apparent ability for graphene to change its properties according to the hydrophilicity of its underlying substrate [10], with the number of layers, and defects [11,12].

Other excellent reviews exist on the topic of functionalizing graphene [13,14]. This review aims to focus specifically on the recently growing field of DNA graphene electronic devices by emphasizing interactions between the two materials and discussing the role of DNA aptamers and DNA nanostructures in sensing small molecules and proteins.

2. Interactions of DNA on graphene

DNA graphene based sensors have recently shown great promise as sensors of small molecules [15], proteins and cells [16,17], as well as for DNA sequencing via graphene nanopores [18]. Recently, aptamer-coated GFET sensors have demonstrated excellent sensitivity for small molecule and protein detection. Similar systems have also been studied with graphene oxide (GO) substrates [19–22]. Understanding the interaction between DNA and graphene is key to developing novel biological devices on conjugated carbon substrates. The primary interaction of DNA and graphene is based on non-covalent π–π stacking shown in Fig. 1 [23].

The non-covalent interactions of DNA and graphene have been well studied by isothermal titration calorimetry [24], computationally [25], and by single molecule force microscopy (SMFS) [26,27], however, some inconsistencies remain regarding the relative order of nucleobase binding strength amongst these sources. Nucleobase π–π stacking gives rise to variation in the electrical response of DNA GFETs [28] and is responsible for DNA nanostructure adsorption on graphene [29]. Base stacking interactions are presumed to be similar on graphene as on bulk graphite, however, the apparent transparency of graphene may lead to radically different surface properties [11,12].

Illafar et al. have recently probed the binding strength of single-stranded DNA (ssDNA) and graphite by single molecule force spectroscopy (SMFS) [27]. In these experiments, thiol-terminated DNA oligomers were attached to a gold-coated atomic force microscopy (AFM) probe that was brought in contact with a graphite surface before being withdrawn (Fig. 2).

Withdrawing the probe from the graphite surface produced steady-state forces connected by abrupt steps, which represent

Please cite this article in press as: N.S. Green, M.L. Norton, Interactions of DNA with graphene and sensing applications of graphene field-effect transistor devices: A review, Anal. Chim. Acta (2014), http://dx.doi.org/10.1016/j.aca.2014.10.023

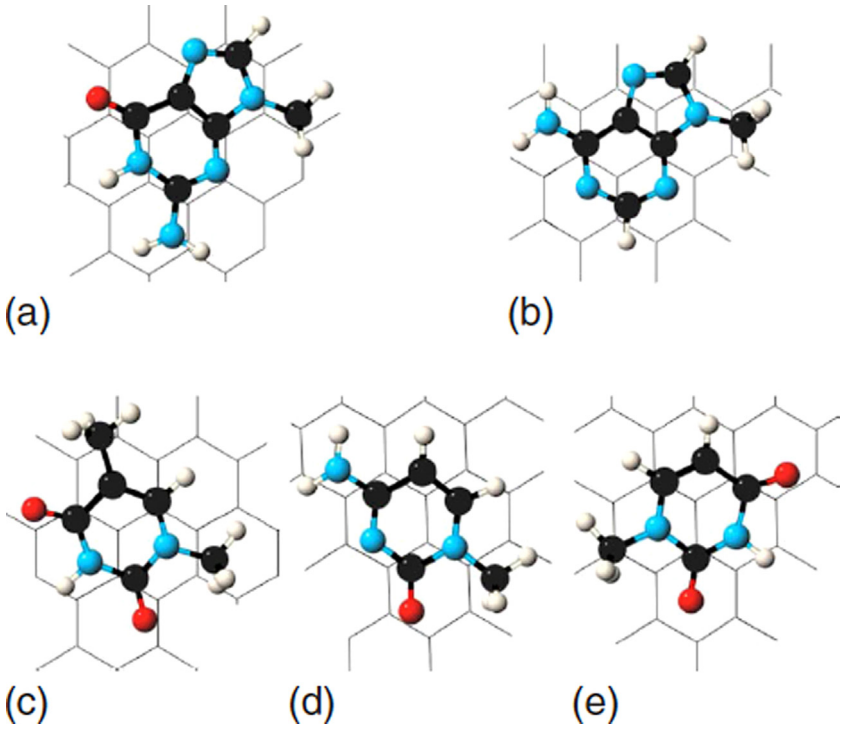

Fig. 1. Equilibrium geometry of nucleobases on top of graphene (a) guanine, (b) adenine, (c) thymine, (d) cytosine, and (e) uracil. Reprinted with permission from [23]. Copyright 2007 American Physical Society.

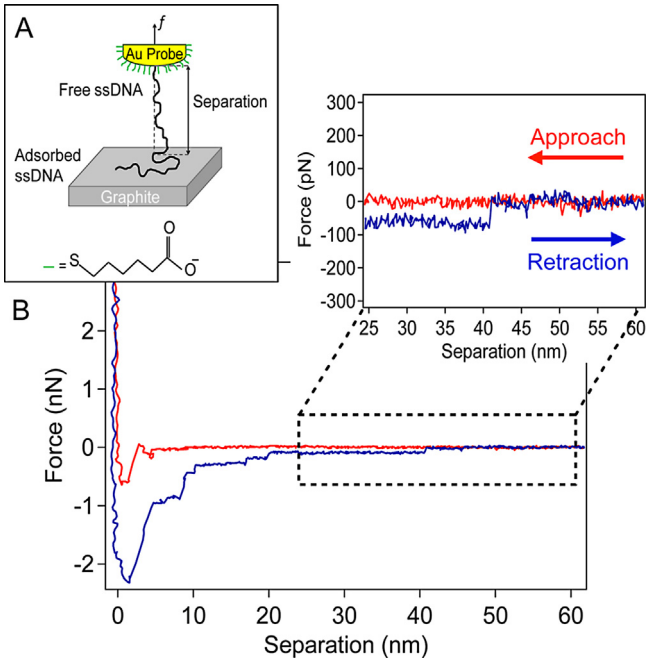

Fig. 2. (A) Idealized cartoon (not drawn to scale) of peeling an ssDNA homopolymer, attached to a gold-coated force probe, from a graphite surface. (B) Typical force–distance curves for peeling 5′-poly(dT100) ssDNA from the surface of graphite obtained at a tip velocity of 200 nm s^{-1} in 10 mM phosphate buffer solution containing 100 mM NaCl. Red curve is approach, blue is retraction. (For interpretation of the references to color in this figure legend, the reader is referred to the web version of this article.)
Reprinted with permission from [27]. Copyright 2012 American Chemical Society.

peeling forces of a small number of polymer molecules from the flat surface. The authors calculated the binding energy per monomer base, 8 – 11 k_BT, from the peeling forces measured in the SMFS experiments. These forces are theoretically strong enough to overcome the base pairing H-bonding forces, ~1 k_BT [30], which would lead to melting upon introduction of double-stranded DNA (dsDNA) to graphite [31].

Density-functional theory calculations have shown that DNA physisorption induces an interfacial dipole between the nucleobases and graphene in addition to π–π stacking [25]. The dipole is the result of the close association of electron-rich aromatic rings of the bases and the polarizable graphene surface (Fig. 3) [32].

The induced dipole from physisorption is important not only for binding energy contribution but also for shifting the minimum conductance at a particular gate voltage ($V_{G,\ min}$), which is commonly studied in DNA graphene field-effect transistor sensors [33]. π–π stacking and electronic interactions (e.g., induced dipoles, doping, and chemical gating) form the primary interactions of DNA based graphene sensors and are important considerations for the application of DNA-based nanostructures.

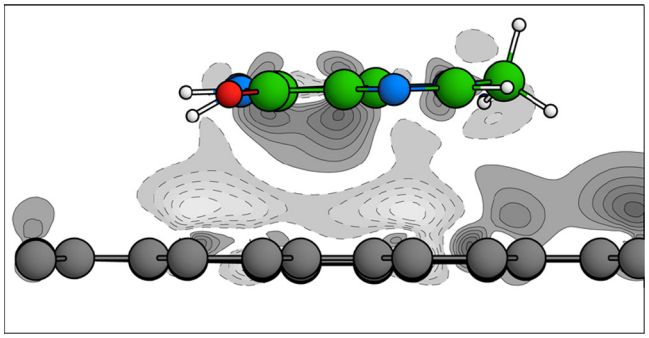

Fig. 3. Calculated charge density difference $\Delta\rho$ for adsorbed G on graphene.
Reprinted with permission from [25]. Copyright 2013 American Chemical Society.

Please cite this article in press as: N.S. Green, M.L. Norton, Interactions of DNA with graphene and sensing applications of graphene field-effect transistor devices: A review, Anal. Chim. Acta (2014), http://dx.doi.org/10.1016/j.aca.2014.10.023

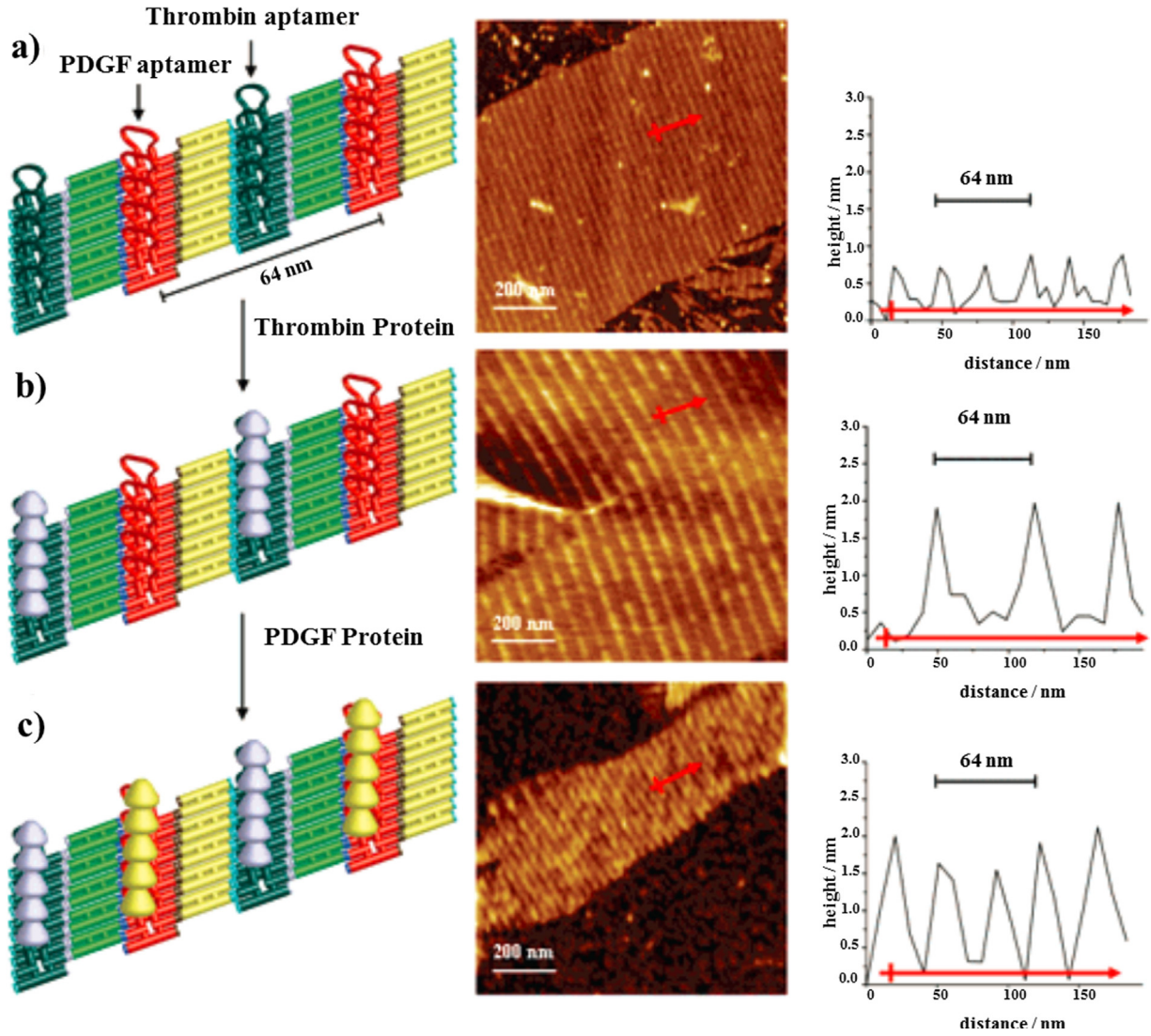

Fig. 4. Periodic 2D multiprotein nanoarrays. (Left) Schematics showing 2D DNA nanoarrays containing alternate thrombin and platelet derived growth factor (PDGF) aptamers and binding of their protein targets. The red and green stem-loops represent the thrombin and PDGF binding aptamers respectively. Grey and yellow balls represent thrombin and PDGF, respectively; (middle) AFM image corresponding to the arrays shown on the left; (right) line cross-section analysis of the AFM images. (For interpretation of the references to color in this figure legend, the reader is referred to the web version of this article.)
Reprinted with permission from [34]. Copyright 2007 American Chemical Society.

3. Structure of DNA origami on graphene

Very little has been published about the nature of DNA nanostructures deposited on graphene despite the potential of combining the nanometer resolution of these materials with the electronic sensitivity of graphene. DNA based nano-structures have previously been shown to capture multiple proteins at discrete locations by placing different DNA-aptamers at alternating locations along linear arrays (Fig. 4) [34,35]. DNA origami, which is another form of DNA nanostructure [36], is produced through the reaction of

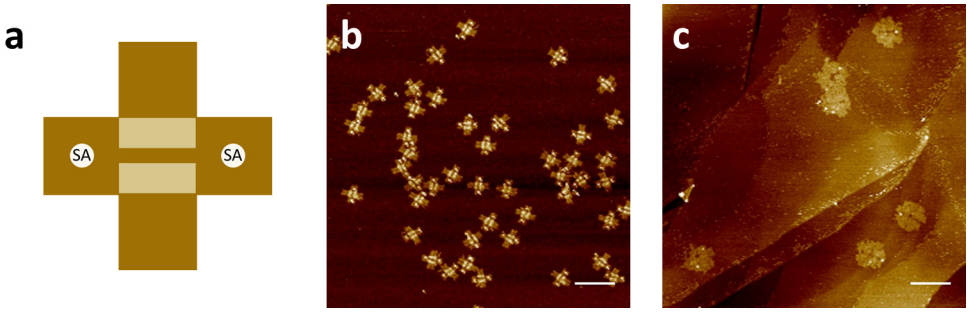

Fig. 5. Deposition of cross-shaped origami from solution onto mica and highly order pyrolytic graphite (HOPG). (a) Schematic representation of cross-shaped origami with streptavidin (SA) protein bound to each arm via biotinylated staples; (b) filtered SA-complexed origami on mica; and (c) filtered SA-complexed origami on HOPG. Note that SA protein can still be seen attached to origami (white dots). Scale bars, 200 nm (AFM lateral); 10 nm (height scale) [90].

Please cite this article in press as: N.S. Green, M.L. Norton, Interactions of DNA with graphene and sensing applications of graphene field-effect transistor devices: A review, Anal. Chim. Acta (2014), http://dx.doi.org/10.1016/j.aca.2014.10.023

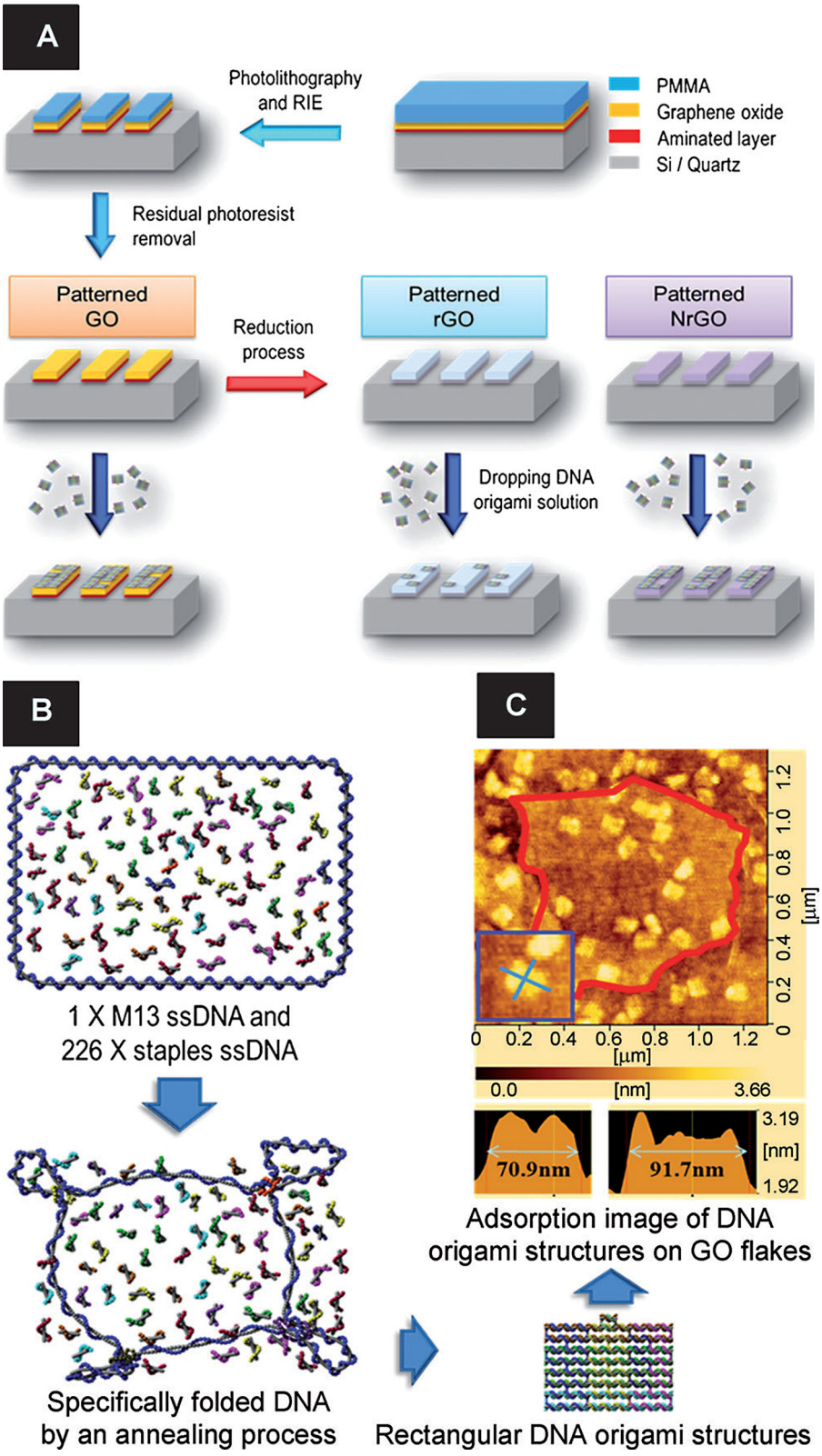

Fig. 6. (A) Patterning of DNA origami structures on graphene-based substrates. Spin-cast GO films are lithographically patterned and chemically modified by reduction or N doping. DNA origami structures were assembled on patterned graphene-based films from buffer solution (RIE = reactive ion etching). (B) A rectangular DNA origami assembly (≈2 nm thick, 70 × 90 nm^2) obtained from the 7249 bp M13 ssDNA template and 226 small ssDNA staples. (C) AFM image and height profile of DNA origami structures on GO flakes. The red solid line shows the boundary of a single GO flake. The inset highlights one DNA origami structure to reveal its cross-sectional dimensions and rectangular shape. (For interpretation of the references to color in this figure legend, the reader is referred to the web version of this article.)
Reprinted with permission from [29]. Copyright 2012 WILEY-VCH Verlag GmbH & Co. KGaA, Weinheim.

large, often circular, strands of ssDNA and shorter 'staple' strands of ssDNA that guide the formation of ~100 nm diameter nanoarchitectures and provide nanometer addressability. These structures have been used to present proteins on their surfaces [37,38].

There is a great potential for DNA nanostructures to be incorporated onto GFET sensors as organizational tools for assembling sensing regions with nanometer resolution. These structures can be grown into 1D arrays with each monomer containing a unique set of aptamers to achieve multiplex sensing [39]. However, further work is needed to investigate the interactions of DNA origami and graphene in order to realize such devices.

The high substrate sensitivity of DNA origami is likely responsible for the lack of literature reports regarding GFETs based on DNA nanostructures. While origami retains its folded structure on mica, silica [40], and a few self-assembled monolayers (SAMs) [41], graphene has been shown to disturb the folded structure of DNA origami due to the strength of the previously discussed π–π stacking interactions [42]. This effect is clearly demonstrated when the same solution of filtered cross-shaped origami [43] are deposited on mica and highly order pyrolytic graphite (HOPG), respectively (Fig. 5).

The nanostructures show morphological disruption when deposited on HOPG. The structures increase their surface area and generally lose the sharp 90° angles which can readily be seen in structures when they are deposited on the compatible mica surface. The cross-shaped origami were prepared with biotinylated staples and complexed with streptavidin (SA) protein as previously described [44]. Importantly, the excess ssDNA 'staple' molecules were removed, via centrifuge membrane columns, from the origami solutions before deposition. Excess DNA in solution can passivate the substrate surface and alter the binding interactions with the nanostructures similar to previously reported coatings with pyrene derivatives [45]. The disruption to the cross-shaped origami structure is a concern for future implementation of these materials on GFET sensors but it is interesting to note that some of the bound protein is still clearly in place in the pseudo-melted nanostructures seen in the HOPG AFM images (Fig. 5c). This would suggest that changes in the morphology of the nanostructures may not necessarily affect sensor viability, but more work is needed to investigate if this holds true for analytes that are added after origami structures have been deposited. Increasing the stability of DNA origami on graphene surfaces is thus an important challenge to address in integrating these structures into GFET devices.

Despite these challenges, Yun et al. have recently reported depositing DNA origami onto chemically modified graphene substrates, including CVD and modified graphene oxide (GO), in finite locations via photolithographic patterning (Fig. 6) [29].

It is interesting to note that X-ray photoelectron spectroscopy (XPS) showed that relatively little Mg^{2+} ions are adsorbed on the surface of CVD graphene when compared to reduced graphene oxide (rGO) and nitrogen doped reduced graphene oxide (NrGO). The presence of Mg^{2+} on the surface may account for the relative abundance of DNA origami on rGO and NrGO surfaces.

DNA origami GFETs present an exciting prospect of high electronic sensitivity and addressability to create very powerful sensors, but these devices face engineering challenges of deposition control, stability, and reproducibility.

4. Sensing DNA with GFETs

DNA GFETs have recently been employed to detect DNA and other biomolecules [14,46] and DNA hybridization [28,47] by monitoring conductivity changes [48], Raman shifts [49], majority carrier density [28], and fluorescence of labeled nucleotides [50]. GFET DNA sensors are unique among other nucleic acid detection

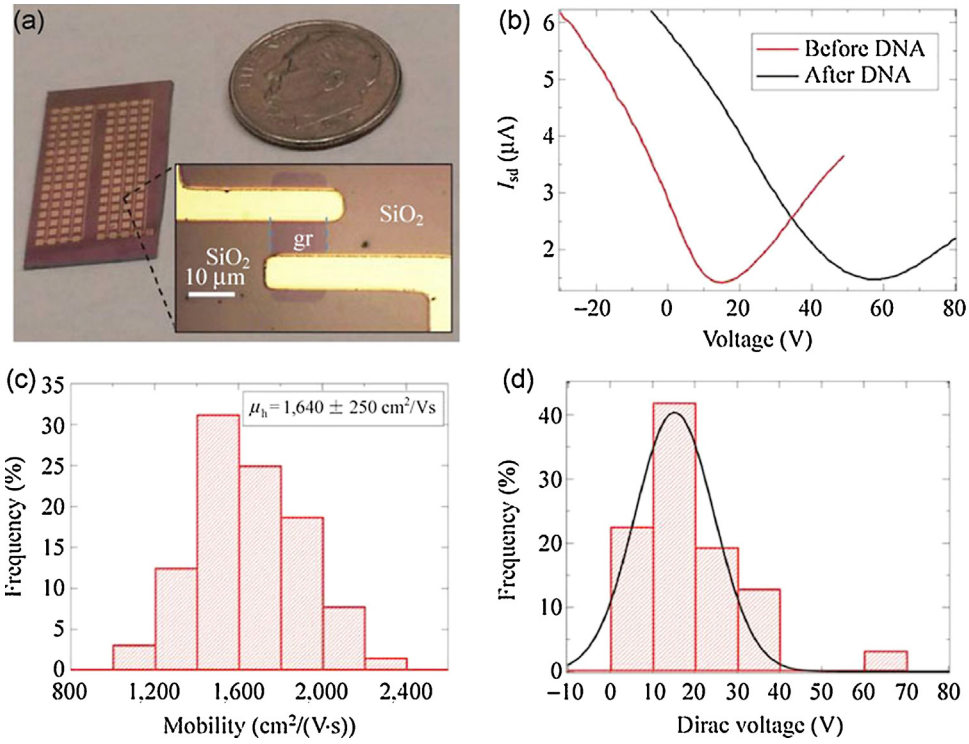

Fig. 7. (a) Dime-sized chips containing 112 devices with channel size 10 μm × 15 μm. (b) I_{sd}–V_G for a typical device with a hole mobility of 1640 $cm^2/(V\,s)$ and Dirac voltage of 14 V. After DNA functionalization, the Dirac voltage is shifted to 58 V. Histograms of (c) hole mobility (corrected for contact resistance) and (d) Dirac voltage, measured in ambient conditions, for typical arrays of 56 devices demonstrate the high quality transistor properties of the graphene devices. The black line is a Gaussian fit to the data. Reprinted with permission from [48]. Copyright 2014 Tsinghua University Press and Springer-Verlag Berlin, Heidelberg.

Please cite this article in press as: N.S. Green, M.L. Norton, Interactions of DNA with graphene and sensing applications of graphene field-effect transistor devices: A review, Anal. Chim. Acta (2014), http://dx.doi.org/10.1016/j.aca.2014.10.023

methods due to their label free detection. This allows for direct detection of oliogonucleotides within a sample without any prior alteration of the sample. These devices can be separated into two different assembly schemes: back-gated and liquid-gated.

4.1. Back-gated GFETs

Back gated GFETs are less frequently employed as DNA sensors, likely due to the difficulties associated with producing devices requiring small gate voltages (V_G) rather than the more commonly and readily prepared higher gate voltage devices, which require V_G on the order of tens to hundreds of volts [51] to achieve significant gain. However, back-gated GFETs have clear sensing advantages over liquid-gated assemblies in conditions in which the analyte solution composition may vary, and in situations where the analyte is not in a solution matrix, e.g., vapor detection [52].

Kybert et al. have recently reported the use of DNA-decorated graphene for arrays of chemical vapor sensors which demonstrated a significant shift in the V_G required to observe the minimum in the device conductance ($V_{G,\,min}$) after DNA deposition [48]. ssDNA was adsorbed onto the surface of graphene, which allowed for chemical vapor sensing down to parts-per-billion as analyte binding further shifted the $V_{G,\,min}$. Fig. 7 shows the device setup, current voltage curves demonstrating the value of $V_{G,\,min}$, which is also termed the Dirac voltage, for the back-gated GFETs before and after the addition of DNA, a mobility histogram and the dispersion of $V_{G,\,min}$ values observed for an array of devices.

These authors explain the positive shift in $V_{G,\,min}$ as counteracting the negative field produced by the phosphate backbone of the adsorbed ssDNA. The gate voltage shifts positive to overcome the negative field induced by DNA in order to maintain a similar charge state for graphene after adsorption. Shifts of $V_{G,\,min}$ in the direction of a more positive gate voltage were previously reported by the same group (Fig. 8) [48].

Generally, back-gated GFETs show relatively large $V_{G,\,min}$ shifts compared to liquid-gate schemes discussed in the next section. Similar electronic principles apply to liquid-gated GFETs but generally require lower potentials compared to back-gated devices.

4.2. Liquid-gated GFETs

Liquid-gated graphene field effect transistors have recently been shown to detect DNA [28], with reported sensitivities down to 0.01 nM and capabilities of detecting single mismatches [47]. The experimental geometry is shown in Fig. 9. A drop of buffer containing the DNA sample is placed onto the surface of a graphene, sheet which has been patterned with source and drain electrodes. The sample solution acts as a gate.

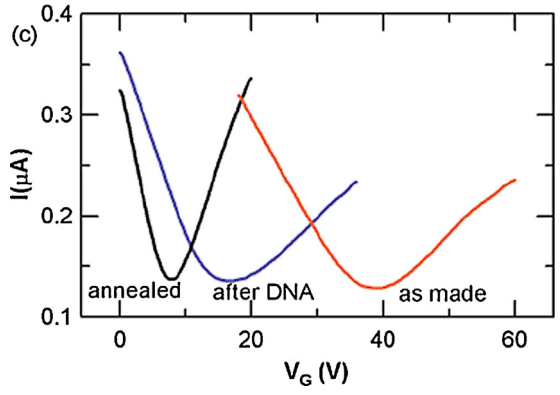

Fig. 8. I–V_G characteristics for a graphene device before (red) and after (black) annealing and after the functionalization step, showing the expected doping shift due to ssDNA application. (For interpretation of the references to color in this figure legend, the reader is referred to the web version of this article.)
Reprinted with permission from [60]. Copyright 2010 AIP Publishing LLC.

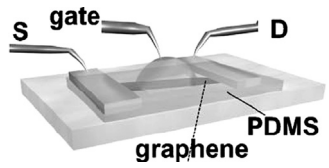

Fig. 9. Schematic diagram of a GFET being operated using liquid gating.
Reprinted with permission of [47]. Copyright 2010 WILEY-VCH Verlag GmbH Co. KGaA, Weinheim.

An important distinction between back- and liquid-gated GFETs is the potential for current to flow between the graphene and the gate electrode via the aqueous ionic solution separating the two conductive bodies. However, gate current leakage is limited, at low gate bias, by the formation of an ionic double layer (Debye layer) formed along the surface of the graphene and gate electrode due to the voltage bias (Fig. 10) [53]. At higher gate bias potentials, the onset of electrolytic processes leads to high gate currents.

Dong et al. recently reported a liquid-gated GFET for detection of DNA hybridization with single base specificity [47]. ssDNA was immobilized on the surface of graphene prior to adding a drop of buffer containing either complimentary or single-base mismatched DNA strands at high concentrations. A silver wire was inserted into the top of the drop to establish the liquid gate. A shift in $V_{G,\,min}$ toward more negative gate potentials (a left shift) was observed upon the addition of DNA to the GFET, which was not attributed to electrostatic gating as previous publications have claimed [54]. Furthermore, the authors were able to rule out the possibility of changes in ionic solution concentration causing the

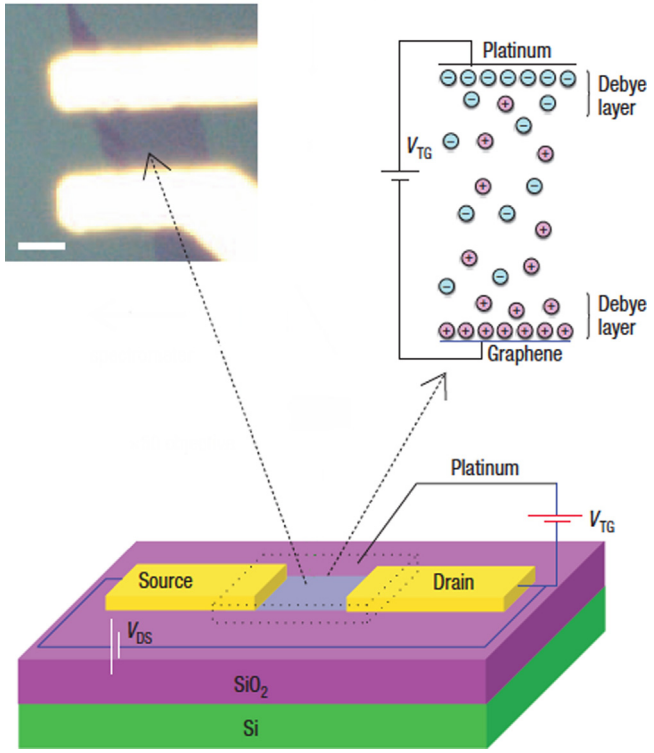

Fig. 10. Formation of a Debye ionic layer formed in a polymer electrolyte gate.
Reprinted with permission from [53]. Copyright 2008 Nature Publishing Group.

left shift [55] by raising the buffer concentration with no observable reversal in $V_{G,\ min}$ (Fig. 11). Others have reported that ionic concentration causes $V_{G,\ min}$ shifts by masking charge impurities in graphene [56,57].

The authors claim that the left shift in $V_{G,\ min}$ is instead due to n-doping by the π–π stacking of electron-rich aromatic rings of the nucleic acids with graphene. Charge injection, or doping, arguments have been previously experimentally discounted from a study that varied the length of charged groups tethered to the surface of a FET sensor [58]. However, a shift of $V_{G,\ min}$ toward more negative bias upon DNA-graphene binding has been explained in the literature by various mechanisms including, p-doping [28,51], n-doping [59], and chemical gating [60].

Lin et al. recently addressed the inconsistency within liquid-gated DNA GFET assemblies. These authors propose that sheet resistance and carrier mobility should be used in lieu of changes in the $V_{G,\ min}$ (the Dirac voltage, or conductance neutral point (V_{CNP})) due to inconsistency between reported measurements [28]. The authors claim that a combination of all three electrical mechanisms (electrostatic gating, graphene doping, and ionic impurity masking) is occurring simultaneously and that the former two are dependent on DNA morphology as demonstrated in Fig. 12.

Phosphate groups are negatively charged chemical gates that shift the $V_{G,\ min}$ toward positive voltage to overcome the opposing

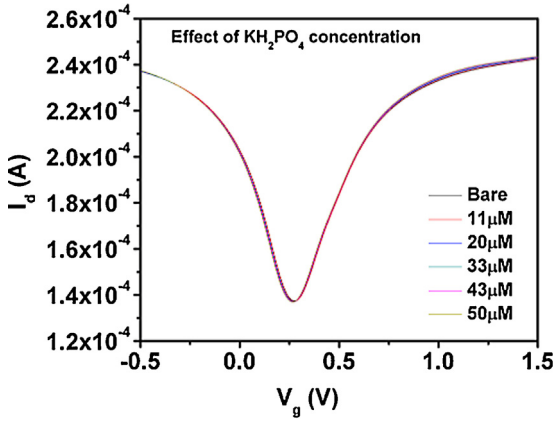

Fig. 11. Increasing phosphate ion concentration did not produce a negative shift in $V_{G,\ min}$.

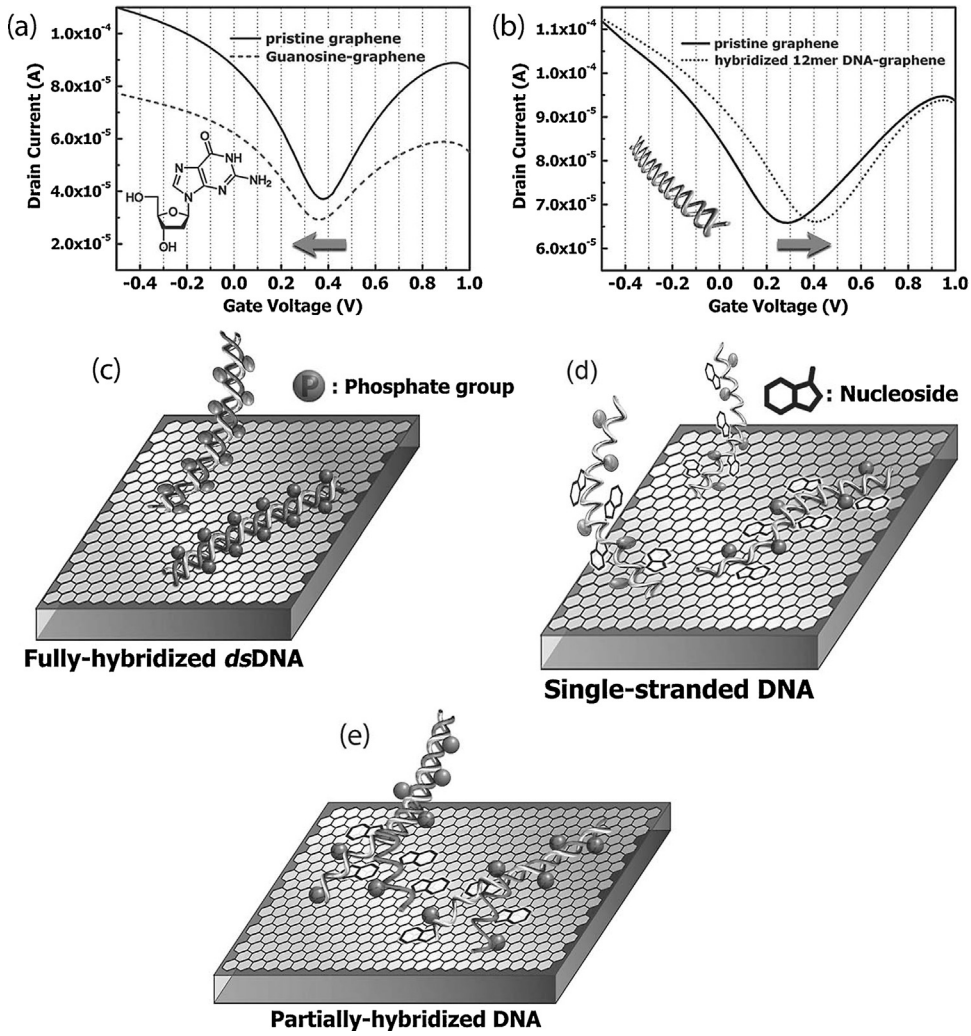

Fig. 12. The transfer curves for a graphene device before and after interacting with (a) the guanosine nucleoside and (b) a dsDNA hybridized from the probe and complementary DNA. Schematic illustration for the interaction between graphene and (c) fully hybridized dsDNA, (d) ssDNA, and (e) partially hybridized DNA. Reprinted with permission from [28]. Copyright 2013 WILEY-VCH Verlag GmbH & Co. KGaA, Weinheim.

Please cite this article in press as: N.S. Green, M.L. Norton, Interactions of DNA with graphene and sensing applications of graphene field-effect transistor devices: A review, Anal. Chim. Acta (2014), http://dx.doi.org/10.1016/j.aca.2014.10.023

Table 1
The change of electrical characteristics of graphene after interacting with nucleosides and various DNA structures.
Reprinted with permission from [28]. Copyright 2013 WILEY-VCH Verlag GmbH & Co. KGaA, Weinheim.

	Nucleosides	Double-stranded DNA	Single-stranded DNA[b]	DNA hybridization (partially hybridized DNA)
Shift of V_{CNP} (electrolyte gating)	Left	Right	Left (most cases)	Left
Hole carrier concentration[a]	Decrease	Increase	Increase (most cases)	Increase

[a] Determined by Hall measurements.
[b] ssDNA sequences available in the original publication's supporting information.

Table 2
Comparison of DNA detection methods.

Detection method	Sensor context	Sensor	LOD	Reference
Hall effect	Graphene field effect transistor (top gate)	Graphene	1 pM	[28]
Gate voltage	Graphene field effect transistor (top gate)	Graphene	0.1 nM	[47]
Colorimetric or fluorescence spectroscopy	Solution	Polythiophene oligonucleotide conjugate	(0.2 μM) 20 fM	[91]
Electrogenerated chemiluminescence	Polypyrrole coated Pt plate	Dye-doped silica nanoparticles oligonucleotide conjugate	0.1 pM	[92]
Homogeneous fluorescence	Solution	Polythiophene–oligonucleotide conjugate	2.4 aM	[93]
Chronopotentiometriy	Polystyrene beads	Ferrocene–oligonucleotide conjugates	5.1 zM	[94]
Electrochemical	Gold/titanium electrode pair	Gold nanoparticle–oligonucleotide conjugate	500 fM	[95]
Electrochemical	Conductive polypyrrole film	Oligonucleotide doped polymer	16 pM	[96]
Electrochemical	Gold nanoparticle decorated electrode	Gold nanoparticle–oligonucleotide conjugate	4.2 pM	[97]
Electrochemical	Conductive ferocenyl polypyrrole electrode	Oligonucleotide doped polymer	2 pM	[98]
Electrochemical impedance spectroscopy	Polypyrrole/MWCNT electrode	Oligonucleotide doped polymer	50 pM	[99]
Electrochemical impedance spectroscopy	Polyaniline/polyacrylate modified diamond electrode	Oligonucleotide doped polymer	20 nM	[100]
Electrochemical impedance spectroscopy	Glassy carbon electrode (GCE)	Biotinylated target oligonucleotide	84.2 nM	[101]
Surface enhanced Raman spectroscopy	Gold nanoparticle	Thiolated oligonucleotide/Raman-tag	100 nM	[102]
Surface enhanced Raman spectroscopy	Gold nanowire	Raman dye-tagged oligonucleotide	10 pM	[103]

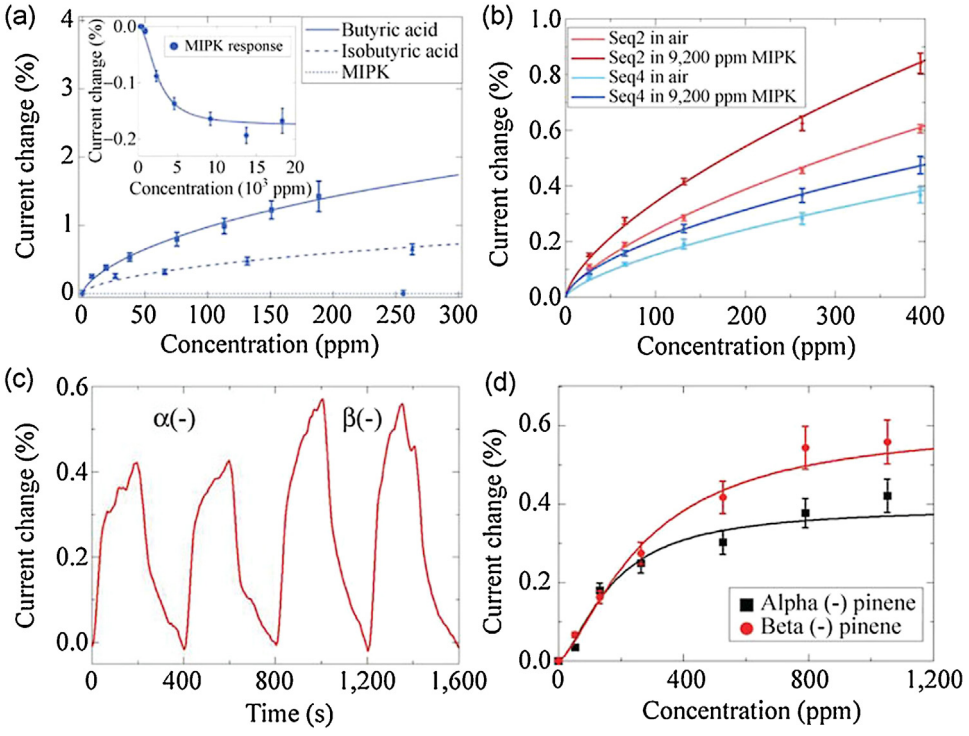

Fig. 13. (a)Device response as a function of concentration of butyric acid, isobutyric acid, and methyl isopropyl ketone (MIPK) for DNA/GFET devices based on Seq3. The carboxylic acid isomers are clearly distinguished, while MIPK is detected only at larger concentrations (inset) and shows a response of opposite sign. (b) Response vs. concentration for DNA/GFET based on Seq2 and Seq4 responding to isobutyric acid in clean air and also in a constant background of 9200 ppm MIPK. Not only is isobutyric acid still detected, but the response magnitude is slightly enlarged, likely due to displacement of MIPK (the binding of which causes a negative response) from the sensor by bound butyric acid. (c) Average response of 5 devices based on Seq2 to 1000 ppm of α(−) and β(−) pinene, repeated twice each. The response to β(−) pinene is reproducibly ~40% larger than the response to α(−) pinene. (d) Responses of DNA/GFET based on Seq2 as a function of concentration for α(−) and β(−) pinene, showing increasing divergence at higher concentrations. Langmuir–Hill fits saturate at 0.39 ± 0.04 and 0.61 ± 0.07 for α(−) and β(−), respectively. The DNA sequences used to modify the surface are provided in the original report.
Reprinted with permission from [48]. Copyright 2014 Tsinghua University Press and Springer-Verlag Berlin, Heidelberg.

Please cite this article in press as: N.S. Green, M.L. Norton, Interactions of DNA with graphene and sensing applications of graphene field-effect transistor devices: A review, Anal. Chim. Acta (2014), http://dx.doi.org/10.1016/j.aca.2014.10.023

field while nucleotides n-dope the graphene surface due to previously discussed π–π stacking. The dsDNA structure thus controls the level of nucleotide doping by lifting the bases off the surface of graphene upon hybridization. Multiple experiments resulted in the following general trends in $V_{G,\ min}$ regarding DNA binding to graphene that are summarized in Table 1.

Discrepancies among literature values for the shifts in the minimum conductivity point and changes in majority carrier characteristics are likely attributable to differences in device and sample design and composition. As device fabrication becomes more standardized, and with increased attention to multiple property characterization of the intrinsic devices, much of the current uncertainty regarding the effect of DNA–graphene binding, changes in DNA morphology, graphene doping and the role of ions in changing the minimum conductivity gate voltage in GFETs will be removed. Despite the current confusion, it is clear that the binding of biomolecules to graphene elicits a measureable electronic response, promising a future of sensitive and label-free DNA detectors.

Table 2 presents the limit of detection (LOD) for a series of DNA sensors based on various experimental/physical methods. GFET sensors display to established methods but are at an advantage in that no prior functionalization of the DNA or the sensors is required. In both GFET cases included in this table, a top-gate was employed as these systems can typically operate under lower gate voltage conditions, which are more compatible with biochemical detection.

5. DNA aptamer-based sensors on graphene

DNA aptamer-based GFET biosensors are highly sensitive, selective, and in at least one report, reusable [15] electronic devices with distinct advantages over previous aptasensor platforms [61]. For example, fluorescent [62] and colorimetric [63] DNA aptamer assays have been demonstrated by utilizing graphene π-stacking to quench a probe upon binding, leaving these devices susceptible to loss of signal through photo-bleaching and chemical fouling [64]. Electronic signaling overcomes these limitations by monitoring current changes in GFETs where no other chemical probes are required as the signal is derived from an analyte being captured on the surface [65]. DNA aptamer GFET sensors have been successfully applied in the detection of species ranging from small molecules to proteins. These two areas will be discussed in turn below. Note that cell detection has also been investigated in similar protein coated GFET sensors [66,67] and in modified graphene and graphene oxide systems [68–70].

5.1. Small molecule sensors

DNA aptamer graphene sensors provide low background signal and high substrate selectivity [65], making these devices well suited for small molecules that are often difficult to detect in complex mixtures of similar species [71].

Kybert et al. recently reported a highly sensitive chemical vapor GFET sensor that is capable of distinguishing between members of a series of low molecular weight organic acids and structural isomers of pinene as shown in Fig. 13 [48].

High binding affinity of the DNA aptamers and low noise from the graphene substrate allowed the device to reach low detection limits (ppm). The authors argue that the high signal seen from carboxylic acid detection is due to a deprotonation that occurs along the nanoscale water layer absorbed to the DNA aptamers as no response was detected from the structurally similar methyl isopropyl ketone (MIPK), which lacks an ionizable proton. A low background signal of a molecular beacon aptamer graphene oxide (GO) device has also been recently reported [72]. Thus, graphene aptasensors are well-suited for discriminating structurally similar, small molecules as well as ions [73].

An et al. describe higher detection limits in GFET devices that have previously been p-doped by employing an oxygen plasma-treated graphene [74]. The authors claim that the increased stability and sensitivity in the p-doped region is the result of electronegative adsorbed oxygen species (O_2 and H_2O) negating the electron density of the n-doped regions [75]. These devices have demonstrated mercury ion detection into picomolar concentrations in the presence of several similar divalent ionic species (Fig. 14).

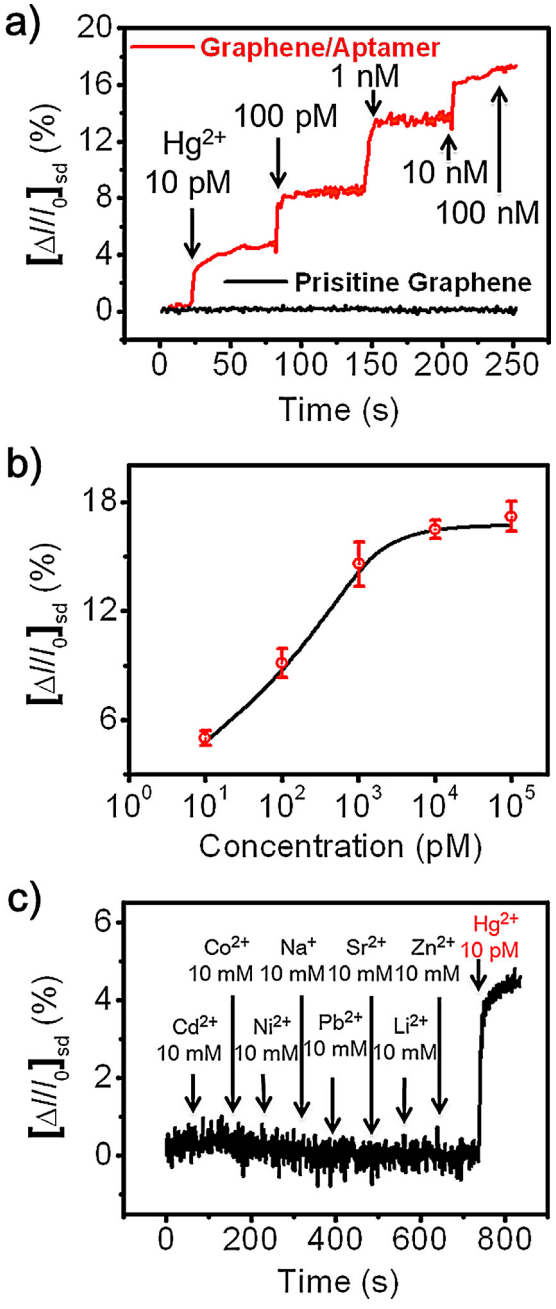

Fig. 14. (a) Real-time responses and (b) calibration curve of the aptasensor with various Hg^{2+} concentrations (10 pM–100 nM). Graphene substrate without aptamer was introduced as a control sample. (c) Selective responses of the aptasensor toward target metal ion (Hg^{2+}, 10 pM) and non-target metal ions (Cd^{2+}, Co^{2+}, Ni^{2+}, Na^{2+}, Pb^{2+}, Sr^{2+}, Li^{2+} and Zn^{2+}, 10 mM).
Reprinted with permission from [74]. Copyright 2013 American Chemical Society.

Table 3
Comparison of small molecule detection methods.

Detection method	Analyte	Analyte condition	Detection parameter	LOD	Reference
Aptamer coated GFET (back gate)	Low mw organics[a]	Vapor	ΔI_{ds}	1 ppm	[48]
Aptamer coated GFET (top gate)	Amyl butyrate	PBS buffer	ΔI_{ds}	0.4 fM	[75]
DNA coated GFET (back gate)	Nonanal	Vapor	I–V_G	0.6 ppm	[104]
Capacitive micromachined ultrasonic transducer (CMUT)	Dimethyl methyl-phosphonate (DMMP)	Vapor	Frequency shift (kHz)	10 ppb	[105]
Aptamer functionalized graphene/two photon (TP) fluorphores	ATP	HEPES/cell growth buffer	Fluorescence intensity	0.5 μM	[64]
Aptamer labeled graphene modified glassy carbon electrode (GCE)	ATP	TMN buffer (determination buffer)	Electrochemical (DPV)	0.3 nM	[65]
Aptamer coated GFET (back gate)	Mercury ions	Acetonitrile	ΔV_G	1.2 μM	[73]
Aptamer coated GFET (top gate)	Mercury ions	PBS buffer	ΔI_{ds}	10 pM	[74]
4-MYP coated Ag nanoparticles	Mercury ions	Tris buffer	SERS	0.34 nM	[106]

[a] Propionic, butyric, hexanoic, and octanoic acids/pinene isomers.

In addition to excellent selectivity, the signal response times were less than 1 s and a practical application of the GFET aptasensor, detecting mercury ions (Hg^{2+}) in mussels, was demonstrated [34]. A similar mercury sensor has also been recently reported using GO [73], which is of increasing interest in biological sensing due to the apparent hydrophobicity of graphene [69,70,76], a property which may limit its solution phase applications. Despite these concerns, protein and cell detection using aptamer-based graphene sensors has been demonstrated [68,77].

Table 3 summarizes the small molecule DNA aptamer GFETs discussed in this section and compares these sensors to previous detection systems for similar analytes. The detection levels vary widely between detection methods due to the complexity of the substrate and the sensing medium. Here, as before, the aptamer GFET sensors are unique in that they require no pre-processing of the target analyte.

5.2. Protein sensors

Sensing proteins with field effect transistors (FETs) is especially challenging given the constraints of complex, high ionic-strength buffered environments that are required for biological species. Ionic solutions form electronic double-layers that effectively lower the apparent charge of biomolecules relative to a surface in a process known as Debye screening [78]. The Debye screening length (λ_D), defined as the length scale between a surface and analyte in which charges on the analyte are screened by counter ions in solution, is highly solution composition dependent [79]. Thus, performance of sensor devices, which bind the analyte close to the sensing substrate have been experimentally demonstrated as more sensitive [80]. This close proximity does not allow ions to form a charge-neutralizing layer between the captured analyte and the sensing substrate. Thus, DNA aptamer sensors are well suited to overcome the Debye screening obstacle in the detection of proteins [68,81,82]. Fig. 15 illustrates the distance dependence of sensing with antibodies compared to aptamers.

Antibodies have been the most widely used species for bimolecular capture, but are not well suited for field-effect applications due to their size. DNA aptamers are significantly smaller in length but have not been as widely implemented as antibodies. Masumoto et al. recently reported a combined aptamer–antibody sensor that avoids Debye screening while still allowing the flexible aptamer to bring captured antibody/antigen complexes near the GFET surface. The combined sensor displayed comparable detection limits to previous fluorescent antibody detection methods without any pre-processing of the sample [83].

Kim et al. recently reported a liquid top-gated aptamer GFET sensor capable of detecting a component of the anthrax toxin protective antigen (PA) in the attomolar range [81]. This device performed well with regard to level of detection (LOD), dynamic detection range, and sensitivity (Fig. 15).

The authors attribute the larger enhancement of signal transduction of the aptamers to larger $V_{G,\ min}$ shifts (30 mV per decade concentration increase), an increase in dynamic range ($I_{ds,\ min}$ increased 1.5–9.5% between 12 aM and 120 fM), and lower LOD (12 aM). All of these parameters out performed similar antibody GFET sensors and electrical silicon nanowire sensor [84]. DNA aptamers are advantageous compared antibody modified sensors because they minimize Debye screening by binding and holding the charged analytes closer to the detection surface (Fig. 16).

Correlation of sensitivity and λ_D has recently been highlighted by Saltzgaber et al. in the detection of thrombin protein in 2-(*N*-morpholino) ethanesulfonic acid (MES) [85]. Here, graphene was first decorated with pyrenebutanoic acid succinimidyl ester (PBASE) in order to increase surface hydrophilicity before attaching thrombin-binding aptamer (TBA) (Fig. 17). Similar surface treatments have been shown with gluteraldehyde-conjugated

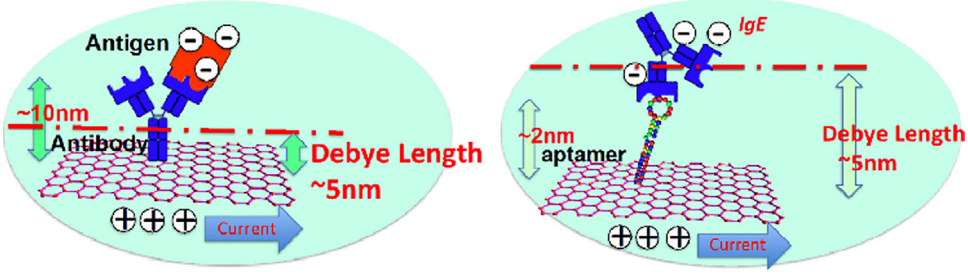

Fig. 15. Depiction of 5 nm Debye screening length on modified graphene surfaces. Left, antibody/antigen reaction in solution. Right, aptamer reaction in solution. Reprinted with permission from [83]. Copyright 2014 IOP Publishing. All rights reserved.

Please cite this article in press as: N.S. Green, M.L. Norton, Interactions of DNA with graphene and sensing applications of graphene field-effect transistor devices: A review, Anal. Chim. Acta (2014), http://dx.doi.org/10.1016/j.aca.2014.10.023

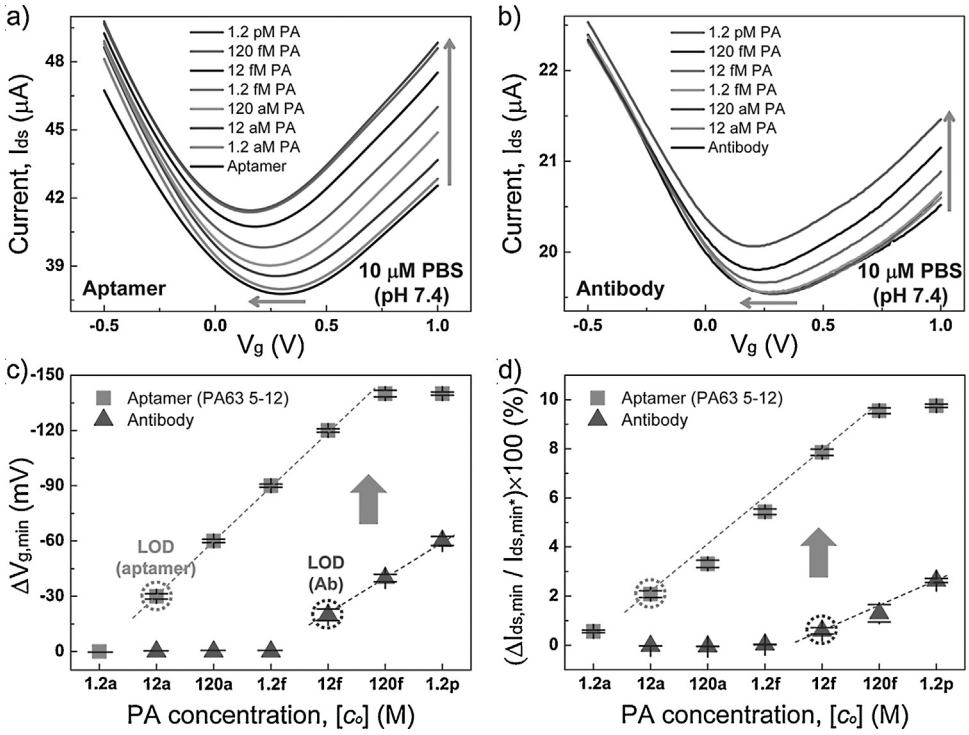

Fig. 16. Transfer characteristics of GFET with (a) aptamer and (b) Ab probe measured at V_{ds} = 0.1 V with varying concentrations of protective antigen (PA) in 10 μM PBS. The transfer characteristics were obtained at 10 min after adding the analyte solution. The isoelectric point (pI) of PA is 5.6. (c) $V_{G,\,min}$ shift ($\Delta V_{G,\,min}$) vs. PA concentration in PBS solutions with different probe molecules. The $\Delta V_{G,\,min}$ value was obtained by calculating the difference in charge neutrality point, $V_{G,\,min}$ as a reference for the device with no binding of PA. (d) The change in the minimum source-drain current ($I_{ds,\,min}$), $\Delta I_{ds,\,min}/I_{ds,\,min}{}^{*} \times 100$ (%) vs. PA concentration. Here, $I_{ds,\,min}{}^{*}$ is the $I_{ds,\,min}$ for the device with no binding of PA.
Reprinted with permission from [81]. Copyright 2013 WILEY-VCH Verlag GmbH & Co. KGaA, Weinheim.

1,5-diaminonapthalene (DAN) as a sensor surface modification before applying an aptamer to detect vascular endothelial growth factor (VGEF), a cancer biomarker [86].

The λ_D for MES buffer of ~20 nm is well-suited for aptamer sensing when compared to phosphate buffered saline (PBS) ($\lambda_D \sim 0.76$ nm), which is problematic in organic field-effect transistors [87]. In these studies, a flow cell was constructed around the graphene to allow rapid introduction and removal of liquid samples from the GFET sensing region. The PBASE coating provided brief but strong binding of thrombin near the sensor

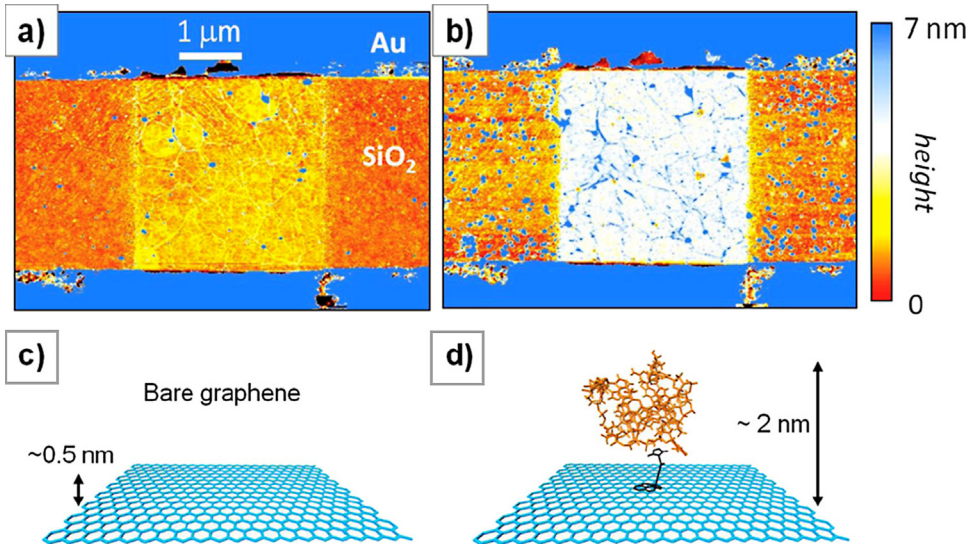

Fig. 17. Functionalization of the graphene surface. (a) Atomic force microscopy image showing the bare graphene channel (3 × 3 μm^2) on an SiO_2 substrate. A pair of gold electrodes are seen at the top and bottom of the image. The color scale represents surface height. The bare graphene surface is ~0.5 nm above the substrate. (b) Atomic force microscopy image of the same device after treating the surface with pyrenebutanoic acid succinimidyl ester (PBASE) and aptamer. The functionalized graphene surface is ~2 nm above the substrate. (c) Illustration of the bare graphene surface, consistent with the first AFM image. (d) Illustration of the functionalized graphene surface showing the molecular structure of PBASE (black) and the molecular structure of the aptamer. The expected size of the PBASE–aptamer construct is consistent with the second AFM image.
Reprinted with permission from [85].

Please cite this article in press as: N.S. Green, M.L. Norton, Interactions of DNA with graphene and sensing applications of graphene field-effect transistor devices: A review, Anal. Chim. Acta (2014), http://dx.doi.org/10.1016/j.aca.2014.10.023

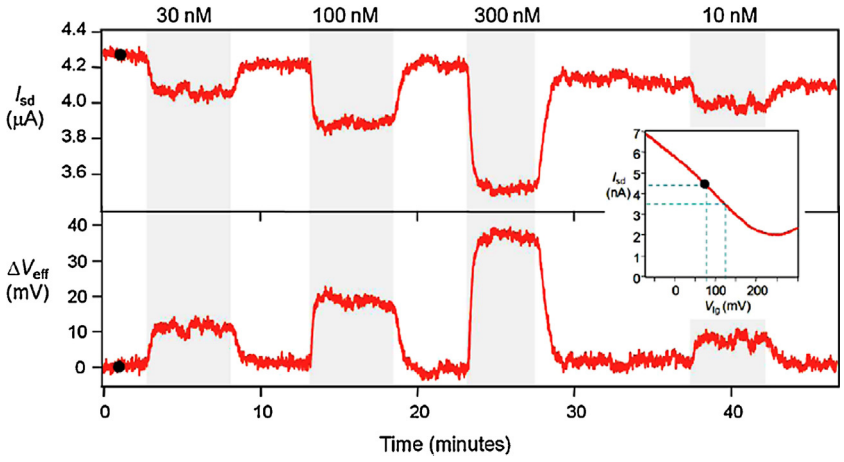

Fig. 18. Protein sensing in real time with an aptamer-based GFET device. The four shaded areas (gray) indicate time periods when the device is exposed to thrombin (30 nM, 100 nM, 300 nM and 10 nM, respectively). The liquid gate is fixed at V_{lg} = 75 mV and a constant flow rate of 25 μL min^{-1} was maintained throughout the experiment. Data points were collected every 0.5 s. The upper panel shows raw $I_{sd}(t)$ data. Drops in I_{sd} occur whenever the device is exposed to thrombin. The lower panel shows the calculated effective gate voltage shift $\Delta V_{eff}(t)$. A baseline drift of 0.21 mV min^{-1} was subtracted from this curve. Directly after thrombin is introduced the rate of change of ΔV_{eff} is 21 mV min^{-1}; 67 mV min^{-1} and 106 mV min^{-1} for 30 nM, 100 nM and 300 nM, respectively. The inset shows I_{sd} (V_{lg}) used to calculate $\Delta V_{eff}(t)$.
Reprinted with permission from [85].

Table 4
Comparison of protein and cell sensors.

Analyte	Detection method	Detection parameter	Analyte condition	LOD	Reference
Protective antigen (anthrax toxin)	Aptamer coated GFET (top gate)	ΔI_{ds}	PBS buffer	1.2 aM	[81]
Protective antigen (anthrax toxin)	Fluorescently labeled antibodies/silver island films	Metal enhanced fluorescence	PBS buffer	15.8 fM	[107]
Thrombin	Aptamer coated GFET (top gate)	ΔI_{ds}	MES buffer	30 nM[a]	[85]
Thrombin	Aptamer coated nanospheres	Electro-chemiluminescence	PBS buffer	0.2 pM	[108]
Thrombin	Aptamer coated Reduced graphene oxide (rGO)	Electrochemical	PBS buffer	0.45 fM	[88]
Immunoglobulin E (IgE)	Aptamer-antibody coated GFET (top gate)	ΔI_{ds}	Phosphate buffer	290 pM	[83]
Immunoglobulin E (IgE)	Aptamer coated MWCNT on glassy carbon electrode (GCE)	Electrochemical (DPV)	PBS	37 pM	[109]
P. falciparum infected erythrocyte (malaria)	Peptide-coated graphene FET	ΔI_{ds}	RPMI 1640 medium	1 cell (flow)	[66]
S. aureus cells	Peptide-coated graphene functionalized silk thin film	Conductivity shift	PBS buffer or direct attachment to solid	1 cell μL^{-1}	[67]
HeLa cells	Aptamer coated graphene	Electrochemical impedance spectroscopy	RPMI 1640 medium	793 cells mL^{-1}	[68]
HeLa cells	Multifunctional aptamers	Chemiluminescence	HEPES buffer	6000 cells mL^{-1}	[110]
K562 cells	Chitosan and carbon nanofiber modified glassy carbon electrode (GCE)	Electrochemical impedance spectroscopy	PBS buffer	1000 cells mL^{-1}	[111]
BGC-823 human gastric carcinoma cells	RGDS tetrapeptide-functionalized SWCNT	Electrochemical impedance spectroscopy	PBS buffer	620 cells mL^{-1}	[112]

[a] Lowest reported detection.

surface, which was shown to be reusable by flowing through MES buffer free of analyte (Fig. 18).

The thrombin aptamer sensor displayed good quantitative binding data, target selectivity, and robust reusability. However, lower detection limits (0.45 fM) have been reported on analogous reduced graphene oxide sensors [88]. Changes in I_{ds} with respect to time were assumed to be the result of surface charge density due to positively charged bound thrombin. The effective gate voltage (ΔV_{eff}) brought on by these charges is proportional to the surface charge density and thus can be used to quantify bound protein and calculate binding kinetics [89]. No signal was detected when the device was introduced to 100 nM streptavidin. Similar binding affinities were seen after the sensor was used, washed and dried with water and N_2 gas, and reused one week later.

DNA GFETs have been shown to be effective protein sensors by overcoming Debye screening effects that limit the utility of larger probes. The low LOD, high dynamic range, and excellent reproducibility of these devices make them well suited for otherwise challenging biological samples. To the best of our knowledge, no DNA aptamer GFET sensors have been reported for detecting cells. However, closely analogous detection schemes, e.g., protein coated GFET sensors, have been reported. Table 4 outlines the protein sensors discussed here as well as some examples of similar cell detection methods and compares all of these methods to previously established protocols.

6. Conclusion and future developments

Aptamer-based graphene field-effect transistors (GFET) combine the sensitive electronics of a unique two-dimensional material with the highly specific probing power of oligonucleotides while minimizing Debye screening and sample preparation issues. Recent advancements in graphene production have made these devices possible and proof-of-concept applications have been demonstrated with small molecules and proteins. However, there is still much to be done as the aptamer-target molecule

Please cite this article in press as: N.S. Green, M.L. Norton, Interactions of DNA with graphene and sensing applications of graphene field-effect transistor devices: A review, Anal. Chim. Acta (2014), http://dx.doi.org/10.1016/j.aca.2014.10.023

interactions and even the structures of the probes themselves are poorly understood.

The interaction of DNA and graphene allows for efficient binding of oligonucleotides to the sensor surface but has been shown to disrupt the hydrogen bonding forces between complementary strands. This is potentially problematic for the use of DNA nanostructure sensors as spatial resolution may be lost. Stabilizing the interaction between DNA nanostructures and graphene is an important problem to address and is an active area of research in our group.

GFET sensors have demonstrated DNA detection limits comparable to previously established methods, however, GFETs have the advantage that no prior sample preparation is required prior to detection. These sensors are based on monitoring changes in the electrical characteristics of these transistors as DNA adsorbs onto the surface of the device. Multiple mechanisms (e.g., doping, electrostatic gating, and buffer effects) have been proposed to explain variation in the signals accompanying DNA adsorption, which has led to uncertainty in the detection process. Despite this uncertainty, it is clear that GFET devices are well suited for DNA detection with similar LODs to established methods.

DNA aptamer coated GFET sensors are sensitive detectors for small molecules and proteins. The devices can be either top- or bottom-gated depending on the application. Top-gated sensors generally require much lower gate voltages (0.1–1 V compared to 10–100 V) but have inherent instability that arises from utilizing ionic solutions as the insulating material. Conversely, back-gated devices often require higher gate voltages but may provide greater sensor stability and allow for straightforward vapor phase detection. Solution-based measurements utilizing these sensors are subject to ionic screening, or Debye screening, which can negate the effect of bringing a charged object near the surface of the graphene layer. The relatively short chain length of DNA aptamers overcomes this challenge faced by larger capture moieties, i.e., antibodies, by maintaining the analyte closer to the graphene surface.

DNA aptamer-based GFET sensors are sensitive and versatile platforms for the detection of DNA, small molecules, and proteins. The strength of adsorption of DNA onto graphene allows for ease of construction while simultaneously presenting challenges for the installation of DNA-based nanostructures. The elucidation of the nature of this interaction should lead to a better understanding of the sensing mechanism behind this novel detection regime, which has the potential to become a new standard bearer for ultrasensitive detection.

Acknowledgements

The authors gratefully acknowledge helpful discussions with Dr. Xiaoning Zhang (Department of Chemistry, UNC, Chapel Hill) and financial support from the Army Research Office MURI W911NF-11-1-0024.

References

[1] L. Gao, G.X. Ni, B. Liu, A.H. Neto, K.P. Loh, Face-to-face transfer of wafer-scale graphene films, Nature 505 (2014) 190–194.
[2] A.K. Geim, Graphene: status and prospectus, Science 324 (2009) 1530–1534.
[3] J. Xia, F. Chen, J. Li, N. Tao, Measurement of quantum capacitance of graphene, Nat. Nanotechnol. 4 (2009) 505–509.
[4] I. Diez-Perez, Z. Li, J. Hihath, C. Zhang, X. Yang, L. Zang, Y. Dai, X. Feng, K. Muellen, N. Tao, Gate-controlled electron transport in coronenes as a bottom-up approach towards graphene transistors, Nat. Commun. 1 (2010) 1–16.
[5] J. Zaumseil, H. Sirringhaus, Electron and ambipolar transport in organic field-effect transistors, Chem. Rev. 107 (2007) 1296–1323.
[6] J. Millman, C.C. Halkias, Electronic Devices and Circuits, International Student Edition, McGraw-Hill, New York, 1967.
[7] D. Reddy, L.F. Register, G.D. Carpenter, S.K. Banerjee, Graphene field-effect transistors, J. Phys. D: Appl. Phys. 22 (2011) .
[8] M. Famulok, Oligonucleotide aptamers that recognize small molecules, Curr. Opin. Struct. Biol. 9 (1999) 324–329.
[9] Y. Huang, X. Chen, Y. Xia, S. Wu, N. Duan, X. Ma, W. Wang, Selection, identificaiton and applicaiton of a DNA aptamer against *Staphylococcus aureus* enterotoxin A, Anal. Methods 6 (2014) 690–697.
[10] J. Rafiee, M. Ji, H. Gullapalli, A.V. Thomas, F. Yavari, Y. Shi, P.M. Ajayan, N. A. Koratkar, Wetting transparency of graphene, Nat. Mater. 11 (2012) 217–222.
[11] R. Raj, S.C. Maroo, E.N. Wang, Wettability of graphene, Nano Lett. 13 (2013) 1509–1515.
[12] C.J. Shih, S. Lin, K.C. Park, Z. Jin, M.S. Strano, D. Blankschtein, Breakdown in the wetting transparency of graphene, Phys. Rev. Lett. 109 (2012) .
[13] V. Georgakilas, M. Otyepka, B.B. Athanasios, V. Chandra, N. Kim, K.C. Kemp, P. Hobza, R. Zboril, K.S. Kim, Functionalization of graphene: covalent and non-covalent approaches, derivatives and applications, Chem. Rev. 112 (2012) 6156–6214.
[14] T. Premkumar, K.E. Geckeler, DNA and Carbon-Based Nanomaterials Preparation and Properties of Their Composites, CRC Press, New York City, 2011.
[15] D. Tang, J. Tang, Q. Li, B. Liu, H. Yang, G. Chen, Target-induced biomolecular release for sensitive aptmaer-based electrochemical detection of small molecules from magenetic graphene, RCS Adv. 1 (2011) 40–43.
[16] W. Wei, X. Pan, D. Li, J. Qian, L. Yin, Y. Pu, S. Liu, Detection of MUC-1 protein and MCF-7 cells based on fluorescence resonance energy transfer from quantum dots to graphene oxide, J. Nanosci. Nanotechnol. 12 (2012) 7685–7691.
[17] P. Zuo, X.J. Li, D.C. Dominguez, B.C. Ye, A PDMS/paper/glass hybrid microfluidic biochip integrated with apter-functionalized graphene oxide nano-biosensors for one-step multiplexed pathogen detection, Lab Chip 13 (2013) 3921–3928.
[18] C. Sathe, X. Zou, J.P. Leburton, K. Schulten, Computational investigation of DNA detection using graphene nanopores, ACS Nano 5 (2011) 8842–8851.
[19] D. Chen, H. Feng, J. Li, Graphene oxide: preparation, functionalization, and electrochemical applications, Chem. Rev. 112 (2012) 6027–6053.
[20] L. Tang, Y. Wang, Y. Liu, J. Li, DNA-directed self-assembly of graphene oxide with applications to ultrasensitive oligonucleotide assay, ACS Nano 5 (2011) 3817–3822.
[21] Y. Wang, L. Tang, Z. Li, Y. Lin, J. Li, In situ simultaneous monitoring of ATP and GTP using a graphene oxide nanosheet-based sensing platform in living cells, Nat. Protoc. 9 (2014) 1944–1955.
[22] L. Tang, H. Chang, Y. Liu, J. Li, Duplex DNA/graphene oxide biointerface: from fundamental understanding to specific enzymatic effects, Adv. Funct. Mater. 24 (2012) 3083–3088.
[23] S. Gowtham, R.H. Schneicher, R. Ahuja, R. Pandey, S.P. Karna, Physisorption of nucleobases on graphene: density-functional calculations, Phys. Rev. B 76 (2007) 1–4 033401.
[24] N. Varghese, U. Mogera, A. Govindaraj, A. Das, P.K. Maiti, A.K. Sood, C.N.R. Rao, Binding of DNA nucleobases and nucleosides with graphene, Chem. Phys. Chem. 10 (2009) 206–210.
[25] J.H. Lee, Y.K. Choi, H.J. Kim, R.H. Scheicher, J.H. Cho, Physisorption of DNA nucleobases on h-BN and graphene: vdW-corrected DFT calculations, J. Phys. Chem. C 117 (2013) 13435–13441.
[26] S. Manohar, A.R. Mantz, K.E. Bancroft, C.Y. Hui, A. Jagota, D.V. Vezenov, Peeling single-stranded DNA from graphite surface to determine oligonucleotide binding energy by force spectroscopy, Nano Lett. 8 (2008) 4365–4372.
[27] S. Iliafar, K. Wagner, S. Manohar, A. Jagota, D. Vezenov, Quantifying interactions between DNA oligomers and graphite surface using single molecule force spectroscopy, J. Phys. Chem. C 116 (2012) 13896–13903.
[28] C.T. Lin, P.T. Loan, T.Y. Chen, K.K. Liu, C.H. Chen, K.H. Wei, L.J. Li, Label-free electrical detection of DNA hybridization on graphene using hall effect measurements: revisiting the sensing mechanism, Adv. Funct. Mater. 23 (2013) 2301–2307.
[29] J.M. Yun, N.K. Kim, J.Y. Kim, D.O. Shin, W.J. Lee, S.H. Lee, M. Lieberman, S.O. Kim, DNA origami nanopatterning on chemically modified graphene, Angew. Chem. Int. Ed. 51 (2013) 912–915.
[30] J.F. Marko, S. Cocco, The micromechanics of DNA, Phys. World 16 (2003) 37–41.
[31] M. Rahman, D. Neff, M.L. Norton, Origami meets graphene: proscpects and perils, in: L. Smith (Ed.), 9th Annual Conference on the Foundations of NanoscienceSnowbird, Utah, 2012.
[32] A.K. Geim, K.S. Novoselov, The rise of graphene, Nat. Mater. 6 (2007) 183–191.
[33] Y. Ohno, K. Maehashi, K. Matsumoto, Label-free biosensors based on aptamer-modified graphene field-effect transistors, J. Am. Chem. Soc. 132 (2010) 18012–18013.
[34] R. Chhabra, J. Sharma, Y. Ke, S. Rinker, S. Lindsay, H. Yan, Spatially addressable multiprotein nanoarrays templated by aptamer-tagged DNA nanoarchitectures, J. Am. Chem. Soc. 129 (2007) 10304–10305.
[35] S. Rinker, Y. Ke, Y. Liu, R. Chhabra, H. Yan, Self-assembled DNA nanostructures for distance-dependent multivalent ligand–protein binding, Nat. Nanotechnol. 3 (2008) 418–422.
[36] P.W.K. Rothemund, Folding DNA to create nanoscale shapes and patterns, Nature 440 (2006) 297–302.
[37] W. Shen, H. Zhong, D. Neff, M.L. Norton, NTA directed protein nanopatterning on DNA origami nanoconstructs, J. Am. Chem. Soc. 131 (2009) 6660–66661.
[38] J. Nangreave, D. Han, Y. Liu, H. Yan, DNA origami: a history and current perspective, Curr. Opin. Chem. Biol. 14 (2010) 608–615.

Please cite this article in press as: N.S. Green, M.L. Norton, Interactions of DNA with graphene and sensing applications of graphene field-effect transistor devices: A review, Anal. Chim. Acta (2014), http://dx.doi.org/10.1016/j.aca.2014.10.023

[39] D. Koirala, P. Shrestha, T. Emura, K. Hidaka, S. Mandal, M. Endo, H. Sugiyama, H. Mao, Single-molecule mechanochemical sensing using DNA oriami nanostructures, Angew. Chem. Int. Ed. 53 (2014) 1–6 (Ahead of print).
[40] M. Pillers, V. Goss, M. Lieberman, Electron-beam lithography and molecular liftoff for directed attachment of DNA nanostructures on silicon: top-down meets bottom-up, Acc. Chem. Res. 47 (2014) 1759–1767.
[41] T. Torring, N.V. Voigt, J. Nangreave, H. Yan, K.V. Gothelf, DNA origami: a quantum leap for self-assembly of complex structures, Chem. Soc. Rev. 40 (2011) 5636–5646.
[42] S. Husale, S. Sahoo, A. Radenovic, F. Traversi, P. Annibale, A. Kis, ssDNA binding reveals the atomic structure of graphene, Langmuir 26 (2010) 18078–18082.
[43] Y. Liu, H. Zhong, R.W. Ang, N.C. Seeman, Crystalline two-dimensional DNA-origami arrays, Angew. Chem. Int. Ed. 50 (2011) 264–267.
[44] T.S. Wu, M. Rahman, M.L. Norton, From nonfinite to finite 1D arrays of origami tiles, Acc. Chem. Res. 47 (2014) 1750–1758.
[45] Z. Jin, W. Sun, Y. Ke, C.J. Shih, L.C. Paulus, Q.H. Wang, B. Mu, P. Yin, M.S. Strano, Metallized DNA nanolithography for encoding and transferring spatial information for graphene patterning, Nat. Commun. 4 (2013) 1663.
[46] Y. Wang, Z. Li, J. Wang, J. Li, Y. Lin, Graphene and graphene oxide: biofunctionalization and applications in biotechnology, Trends Biotechnol. 29 (2011) 205–212.
[47] X. Dong, Y. Shi, W. Huang, P. Chen, L.J. Li, Electrical detection of DNA hybridization with single-base specificity using transistors based on CVD-grown graphene sheets, Adv. Mater. 22 (2010) 1649–1653.
[48] N.J. Kybert, G.H. Han, M.B. Lerner, E.N. Dattoli, A. Esfandiar, A.T.C. Johnson, Scalable arrays of chemical vapor sensors based on DNA-decorated graphene, Nano Res. 7 (2014) 95–103.
[49] A.N. Sidorov, T.M. Orlando, Monolayer graphene platform for the study of DNA damage by low-energy electron irradiation, Phys. Chem. Lett. 4 (2013) 2328–2333.
[50] C.H. Lu, H.H. Yang, C.L. Zhu, X. Chen, G.N. Chen, A graphene platform for sensing biomolecules, Angew. Chem. Int. Ed. 48 (2009) 4785–4787.
[51] N. Mohanty, V. Berry, Graphene-based single-bacterium resolution biodevice and DNA transistor: interfacing graphene derivatives with nanoscale and microscale biocomponents, Nano Lett. 8 (2008) 4469–4476.
[52] Y. Dan, Y. Lu, N.J. Kybert, Z. Luo, A.T.C. Johnson, Intrinsic response of graphene vapor sensors, Nano Lett. 9 (2009) 1472–1475.
[53] A. Das, S. Pisana, B. Chakraborty, S. Piscanec, S.K. Saha, U.V. Waghmare, K.S. Novoselov, H.R. Krishnamurthy, A.K. Geim, A.C. Ferrari, A.K. Sood, Monitoring dopants by Raman scattering in an electrochemically top-gated graphene transistor, Nat. Nanotechnol. 3 (2009) 210–215.
[54] A.B. Artyukhin, M. Stadermann, R.W. Friddle, P. Stroeve, O. Bakajin, A. Noy, Controlled electrostatic gating of carbon nanotube FET devices, Nano Lett. 6 (2006) 2080–2085.
[55] F. Chen, Q. Qing, J. Li, N. Tao, Electrochemical gate-controlled charge transport in graphene in ionic liquid and aqueous solution, J. Am. Chem. Soc. 131 (2009) 9908–9909.
[56] F. Chen, J. Xia, N. Tao, Ionic screening of charged-impurity scattering in graphene, Nano Lett. 9 (2009) 1621–1625.
[57] Y.Y. Wang, P.J. Burke, A large-area and contamination-free graphene transistor for liquid-gated sensing applications, Appl. Phys. Lett. 103 (2013) 1–4 052103.
[58] M.B. Lerner, J.M. Resczanski, A. Amin, R.R. Johnson, J.I. Goldsmith, A.T.C. Johnson, Toward quantifying the electrostatic transduction mechanism in carbon nanotube molecular sensors, J. Am. Chem. Soc. 134 (2012) 14318–14321.
[59] Z. Yin, Q. He, X. Huang, J. Zhang, S. Wu, P. Chen, G. Lu, P. Chen, Q. Zhang, Q. Yan, H. Zhang, Real-time DNA detection using Pt nanoparticle-decorated reduced graphene oxide field-effect transistors, Nanoscale 4 (2012) 293–297.
[60] Y. Lu, B.R. Goldsmith, N.J. Kybert, A.T.C. Johnson, DNA-decorated graphene chemical sensors, Appl. Phys. Lett. 97 (2010) .
[61] H. Huang, X. Dong, Y. Shi, C.M. Li, L.J. Li, P. Chen, Nanoelectronic biosensors based on CVD grown graphene, Nanoscale 2 (2010) 1485–1488.
[62] H. Zhao, M. Gao, Y. Chang, X. Fan, X. Quan, Fluorescent assay for oxytetracycline based on a long-chain aptamer assembled onto reduced graphene oxide, Microchim. Acta 180 (2013) 829–835.
[63] Y.S. Kim, J.H. Kim, I.A. Kim, S.J. Lee, J. Jurng, M.B. Gu, A novel colorimetric aptasensor using gold nanoparticle for a highly sensitive and specific detection of oxytetracycline, Biosens. Bioelectron. 26 (2010) 1644–1649.
[64] M. Yi, S. Yang, Z. Peng, C. Liu, J. Li, W. Zhong, R. Yang, W. Tan, Two-photon graphene oxide/aptamer nanosensing conjugate for in vitro or in vivo molecular probing, Anal. Chem. 86 (7) (2014) 3548–3554.
[65] W. Wen, J. Bao, M.Z. Zhang, W. Chen, H.Y. Xiong, X.H. Zhang, Y.D. Zhao, S.F. Wang, A novel amperometric adenosine triphosphate biosensor byimmobilizing graphene/dual-labeled aptamers complex ontopoly (o-phenylenediamine) modified electrode, Sens. Actuators B: Chem. 191 (2014) 695–702.
[66] P.K. Ang, A. Li, M. Jaiswal, Y. Wang, H.W. Hou, J.T.L. Thong, C.T. Lim, K.P. Loh, Flow sensing of single cell by graphene transistor in a microfluidic channel, Nano Lett. 11 (2011) 5240–5246.
[67] M. Mannoor, H. Tao, J.D. Clayton, A. Sengupta, D.L. Kaplan, R.R. Naik, N. Verma, F.G. Omenetto, M.C. McAlpine, Graphene-based wireless bacteria detection on tooth enamel, Nat. Commun. 3 (2012) 1767/1761–1767/1768.
[68] L. Feng, Y. Chen, J. Ren, X. Qu, A graphene functionalized electrochemical aptasensor for selective label-free detection of cancer cells, Biomaterials 32 (2011) 2930–2937.
[69] Y. Wang, Z. Li, T.J. Weber, D. Hu, C.T. Lin, J. Li, Y. Lin, In situ live cell sensing of multiple nucleotides exploiting DNA/RNA aptamers and graphene oxide nanosheets, Anal. Chem. 85 (2013) 6775–6782.
[70] Y. Wang, Z. Li, D. Hu, C.T. Lin, J. Li, Y. Lin, Aptamer/graphene oxide nanocomplex for in situ molecular probing in living cells, J. Am. Chem. Soc. 132 (2010) 9274–9276.
[71] K. Mannerstedt, A.M. Jansson, J. Weadge, O. Hindsgaul, Small-molecule sensing: a direct enzyme-linked immunosorbent assay for the monosaccharide Kdo, Angew. Chem. Int. Ed. 49 (2010) 8173–8176.
[72] Y. He, Z.G. Wang, H.W. Tang, D.W. Pang, Low background signal platform for the detection of ATP: when a molecular aptamer beacon meets graphene oxide, Biosens. Bioelectron. 29 (2011) 76–81.
[73] E. Sharon, X. Liu, R. Freeman, O. Yehezkeli, I. Willner, Label-free analysis of thrombin or Hg^{2+} ions by nucleic acid-functionalized graphene oxide matrices assembled on field-effect transistors, Electroanalysis 25 (2013) 851–856.
[74] J.H. An, S.J. Park, O.S. Kwoon, J. Bae, J. Jang, High-performance flexible graphene aptasensor for mercury detection in mussels, ACS Nano 7 (2013) 10563–10571.
[75] S.J. Park, O.S. Kwon, S.H. Lee, H.S. Song, T.H. Park, J. Jang, Ultrasensitive flexible graphene based field-effect transistor (FET)-type bioelectronic nose, Nano Lett. 12 (2010) 5082–5090.
[76] Y. Pu, Z. Zhu, D. Han, H. Liu, J. Liao, K. Zhang, W. Tan, Insulin-binding aptamer-conjugated graphene oxide for insulin detection, Analyst 136 (2011) 4138–4140.
[77] H. Chang, L. Tang, Y. Wang, J. Jiang, J. Li, Graphene fluorescence resonance energy transfer aptasensor for the thrombin detection, Anal. Chem. 82 (2010) 2341–2346.
[78] E. Stern, R. Wagner, F.J. Sigworth, R. Breaker, T.M. Fahmy, M.A. Reed, Importance of the debye screening length on nanowire field effect transistor sensors, Nano Lett. 7 (2007) 3405–3409.
[79] R.B. Schoch, J. Han, P. Renaud, Transport phenomena in nanofluidics, Rev. Mod. Phys. 80 (2008) 839–883.
[80] A. Vacic, J.M. Criscione, N.R. Rajan, E. Stern, T.M. Fahmy, M.A. Reed, Determination of molecular configuration by debye length modulation, J. Am. Chem. Soc. 133 (2011) 13886–13889.
[81] D.J. Kim, H.C. Park, I.Y. Sohn, J.H. Jung, O.J. Yoon, J.S. Park, M.Y. Yoon, N.E. Lee, Electrical graphene aptasensor for ultra-sensitive detection of anthrax toxin with amplified signal transduction, Small 9 (2013) 3352–3360.
[82] Y. Xiao, Y. Wang, M. Wu, X. Ma, X. Yang, Graphene-based lysozyme binding aptamer nanocomposite for label-free and sensitive lysozyme sensing, J. Electroanal. Chem. 702 (2013) 49–55.
[83] K. Masumoto, K. Maehashi, Y. Ohno, K. Inoue, Recent advances in functional graphene biosensors, J. Phys. D: Appl. Phys. 47 (2014) 1–6.
[84] G.J. Zhang, Y. Ning, Silicon nanowire biosensor and its applications in disease diagnostics: a review, Anal. Chim. Acta 749 (2012) 1–15.
[85] G. Saltzgaber, P. Wojcik, T. Sharf, M.R. Leyden, J.L. Wardini, C.A. Heist, A.A. Adenuga, V.T. Remcho, E.D. Minot, Scalable graphene field-effect sensors for specific protein detection, Nanotechnology 355502 (2013) 5.
[86] O.S. Kwon, S.J. Park, J.Y. Hong, A.R. Han, J.S. Lee, J.S. Lee, J.H. Oh, J. Jang, Flexible FET-type VEGF aptasensor based on nitrogen-doped graphene converted from conducting polymer, ACS Nano 6 (2012) 1486–1493.
[87] L. Kergoat, B. Piro, M. Berggren, M.C. Pham, A. Yassar, G. Horowitz, DNA detection with a water-gated organic field-effect transistor, Org. Electron. 13 (2012) 1–6.
[88] Y. Wang, Y. Xiao, X. Ma, N. Li, X. Yang, Label-free and sensitive thrombin sensing on a molecularly grafted aptamer on graphene, Chem. Commun. 48 (2012) 738–740.
[89] B.Y. Lee, M.G. Sung, J. Lee, K.Y. Baik, Y.K. Kwon, M.S. Lee, S. Hong, Universal parameters for carbon nanotube network-based sensors: can nanotube sensors be reproducible? ACS Nano 5 (2011) 4373–4379.
[90] N.S. Green, P.H. Pham, D.T. Crow, P.J. Burke, M.L. Norton, Graphene deposited on mica induces morphological changes in DNA origami (2014) (submitted for publication).
[91] H.A. Ho, M. Boissinot, M.G. Bergeron, G. Corbeil, K. Dore, D. Boureau, M. Leclerc, Colorimetric and fluorometric detection of nucleic acids using cationic polythiophene derivatives, Angew. Chem. Int. Ed. 41 (2002) 1548–1551.
[92] Z. Chang, J. Zhou, K. Zhao, N. Zhu, P. He, Y. Fang, Ru(bpy)-doped silica nanoparticle DNA probe for the electrogenerated chemiluminescence detection of DNA hybridization, Electrochim. Acta 52 (2006) 575–580.
[93] K. Doré, S. Dubus, H. Ho, I. Lévesque, M. Brunette, G. Corbeil, M. Boissinot, G. Boivin, M. Bergeron, D. Boudreau, M. Leclerc, Fluorescent polymeric transducer for the rapid, simple, and specific detection of nucleic acids at the zeptomole level, J. Am. Chem. Soc. 126 (2004) 4240–4244.
[94] J. Wang, R. Polsky, A. Merkoci, K.L. Turner, Electroactive beads for ultrasensitive DNA detection, Langmuir 19 (2003) 989–991.
[95] S.J. Park, A.T. Taton, C.A. Mirkin, Array-based electrical detection of DNA with nanoparticle probes, Science 295 (2002) 1503–1506.
[96] E. Komarova, M. Aldissi, A. Bogomolova, Direct electrochemical sensor for fast reagent-free DNA detection, Biosens. Bioelectron. 21 (2005) 182–189.
[97] K. Zhang, Y. Zhang, Lable-free electrochemical DNA sensor based on gold nanoparticles/poly(neutral red) modified electrode, Electroanalysis 22 (2010) 673–679.

Please cite this article in press as: N.S. Green, M.L. Norton, Interactions of DNA with graphene and sensing applications of graphene field-effect transistor devices: A review, Anal. Chim. Acta (2014), http://dx.doi.org/10.1016/j.aca.2014.10.023

[98] H. Korri-Youssoufi, B. Markrouf, Electrochemical biosensing of DNA hybridization by ferrocenyl groups functionalized polypyrrole, Anal. Chim. Acta 469 (2002) 85–92.
[99] Y. Xu, H. Cai, P.G. He, Y.Z. Fang, Electrochemical impedance detection of DNA hybridization based on the formation of M-DNA on polypyrrole/carbon nanotube modified electrode, Anal. Chim. Acta 516 (2004) 19–27.
[100] H. Gu, X. di Su, K.P. Loh, Electrochemical impedance sensing of DNA hybridization on conducting polymer film-modified diamond, J. Phys. Chem. B 109 (2005) 13611–13618.
[101] A. Bonanni, M.J. Esplandiu, M. del Valle, Signal amplification for impedimetric genosensing using gold-streptavidin nanoparticles, Electrochim. Acta 53 (2008) 4022–4029.
[102] L. Sun, C. Yu, J. Irudayaraj, Surface-enhanced Raman scattering based nonfluorescent probe for multiplex DNA detection, Anal. Chem. 79 (2007) 3981–3988.
[103] T. Kang, S.M. Yoo, I. Yoon, S.Y. Lee, B. Kim, Pattered multiplex pathogen DNA detection by Au particle-on-wire SERS sensor, Nano Lett. 10 (2010) 1189–1193.
[104] Y. Lu, B.R. Goldsmith, N.J. Kybert, A.T.C. Johnson, DNA-decorated graphene chemical sensors, Appl. Phys. Lett. 97 (2010) 83170.
[105] H.J. Lee, K.K. Park, M. Kupnik, O. Oralkan, B.T. Kuhri-Yakib, Chemical vapor detection using a capacitive micromachined ultrasonic transducer, Anal. Chem. 83 (2011) 9314–9320.
[106] L. Chen, N. Qi, X. Wang, L. Chen, H. You, J. Li, Ultrasensitive surface-enhanced Raman scattering nanosensor for mercury ion detection based on functionalized silver nanoparticles, RSC Adv. 4 (2014) 15055–15060.
[107] A.I. Dragan, M.T. Albrecht, R. Pavlovic, A.M. Keane-Myers, C.D. Geddes, Ultrafast pg/ml anthrax toxin (protective antigen) detection assay based on microwave accelerated metal-enhanced fluorescence, Anal. Biochem. 425 (2012) 54–61.
[108] Y.M. Liu, J.J. Zhang, G.F. Shi, M. Zhou, Y.Y. Liu, K.J. Huang, Y.H. Chen, Label-free electrochemiluminescence aptasensor using Ru(bpy) functionalized dopamine melanin colloidal nanospheres and gold nanoparticles as signal-amplifying tags, Electrochim. Acta 129 (2014) 222–228.
[109] S. Khezrian, A. Salimi, H. Teymourian, R. Hallaj, Label-free electrochemical IgE aptasensor based on covalent attachment of aptamer onto multiwalled carbon nanotubes/ionic liquid/chitosan nanocomposite modified electrode, Biosens. Bioelectron. 43 (2013) 218–225.
[110] T. Li, L. Shi, E. Wang, S. Dong, Multifunctional G-quadruplex aptamers and their application to protein detection, Chem. Eur. J. 15 (2009) 1036–1042.
[111] C. Hao, L. Ding, X. Zhang, H. Ju, Biocompatible conductive architecture of carbon nanofiber-doped chitosan prepared with controllable electrodeposition for cytosensing, Anal. Chem. 79 (2007) 4442–4447.
[112] W. Cheng, L. Ding, J. Lei, S. Ding, H. Ju, Effective cell capture with tetrapeptide-functionalized carbon nanotubes and dual signal amplification for cytosensing and evaluation of cell surface carbohydrate, Anal. Chem. 80 (2008) 3867–3872.

Please cite this article in press as: N.S. Green, M.L. Norton, Interactions of DNA with graphene and sensing applications of graphene field-effect transistor devices: A review, Anal. Chim. Acta (2014), http://dx.doi.org/10.1016/j.aca.2014.10.023